Pergamon

Deep-Sea Research I, Vol. 43, No. 2, pp. 159–192, 1996

S0967–0637(96)00012–X
0967–0637/96 $15.00 + 0.00

Seasonal temperature and salinity fields in the Mediterranean Sea: Climatological analyses of a historical data set

P. BRASSEUR,*† J. M. BECKERS,*‡ J. M. BRANKART* and R. SCHOENAUEN*

(*Received* 29 *July* 1994; *in revised form* 3 *March* 1995; *accepted* 11 *September* 1995)

Abstract—Climatological analyses of a historical data base have been carried out with the aim of reconstructing the three-dimensional temperature and salinity fields in the Mediterranean Sea. Seasonal and monthly distributions of hydrographic properties have been computed by a variational inverse method as an alternate to the standard Gandin (1969; Objective analysis of meterological fields, Israeli Program for Scientific Translation, Jerusalem) procedure. The spline solutions of the minimization problem are demonstrated to be numerically and theoretically equivalent to field estimates obtained by conventional objective analysis. The application of a finite-element technique allows analysis to be performed in the model space rather than in the observational space, which substantially improves the numerical efficiency of the procedure. The parameters of the scheme are adjusted according to the statistics of the climatological data. The results, realized as gridded data sets (horizontal resolution of 0.25°), show some trends in seasonal variability affecting the properties of water masses. As expected, the upper layer is subject to a well-defined seasonal signal affecting both the temperature and salinity fields. Error maps, reflecting the degree of uncertainty in the analyses, have been systematically produced. The present work is conceived as a basic support to more advanced studies such as diagnostic calculations, initialization of dynamical models, assimilation of hydrological data into primitive equation models, or planning of experimental surveys. New versions of the climatological fields will be released as data are added to the historical data base. Copyright © 1996 Elsevier Science Ltd.

1 INTRODUCTION

Since the beginning of this century, the Mediterranean Sea has been the site of a continuous effort from the oceanographic community to improve the understanding of the circulation, production, transformation and spreading of the water masses, and to identify the associated forcing mechanisms. As a result of the numerous Mediterranean surveys achieved so far, a huge amount of experimental data has been collected, either for regional or for basin-scale studies. One of the most traditional ways to examine this collection of observations lies in the production of synthetic maps of hydrological properties, depicting the "mean" climatological state of the sea for instance. Of course, such analyses do not reflect the interannual variability of the system but, instead, provide a reference basis for comparison with more focused pictures of the system.

* Université de Liège, GeoHydrodynamics and Environmental Research (GHER), Sart Tilman B5, B-4000 Liège, Belgium.

† Present address: LEGI/IMG, URA 1509 du CNRS, BP 53X, F-38041 Genoble, France.

‡ Senior Research Assistant, National Fund for Scientific Research, Belgium.

The compilation of hydrological charts in atlas form has been the subject of several works on the Mediterranean Sea. Ovchinnikov *et al.* (1976) released a pioneer study, in which climatological analyses of hydrographic data formed the basis of geostrophic calculations. The leading objective was then to identify the dominant hydrodynamic regimes in the Mediterranean. More recently, Guibout (1987) selected a number of high-quality surveys to reconstruct the typical structures observed in the sea; however, the charts contained in this atlas are mostly based on quasi-synoptic information (relevant to the particular periods of the retained cruises); the climatological character of this hydrology may therefore be questioned. Picco (1990) initiated a fully climatological study, considering nearly 15,000 hydrographic casts gathered from various sources. The data set was representative of the period 1909–1987, but it covered the western basin only.

As a subset of his well-known atlas of the world ocean, Levitus (1982) has provided the oceanographic community with the first numerical version of a climatology from which the Mediterranean domain can be isolated (Fig. 1). The general tendencies of the hydrology can be moderately well identified from the Levitus atlas. However, the parameters of the procedure used to analyse the raw historical data in the Mediterranean region do not differ significantly from those used over the global ocean, so that the spatial resolution is not really consistent with the regional scale of the general circulation. There are numerous observations (e.g. La Violette, 1994) indicating that the general circulation develops over smaller scales than those depicted in Fig. 1. For example, the Rossby radius of deformation in the Mediterranean is much smaller than in the world ocean, not exceeding 15 km. A similar lack of resolution can be formulated about the analyses found in Picco (1990).

The need for a numerical atlas, adapted to the scales of the processes under consideration, has recently increased as a result of the many field programs taking place in the Mediterranean. It is often argued that a synergistic approach based on both modelling and experimental skills is the only chance of success for contemporary oceanographers (e.g. Millot, 1994). On the other hand, the processes observed in the Mediterranean display some similarities with those present in the global ocean, but they extend over regions which are

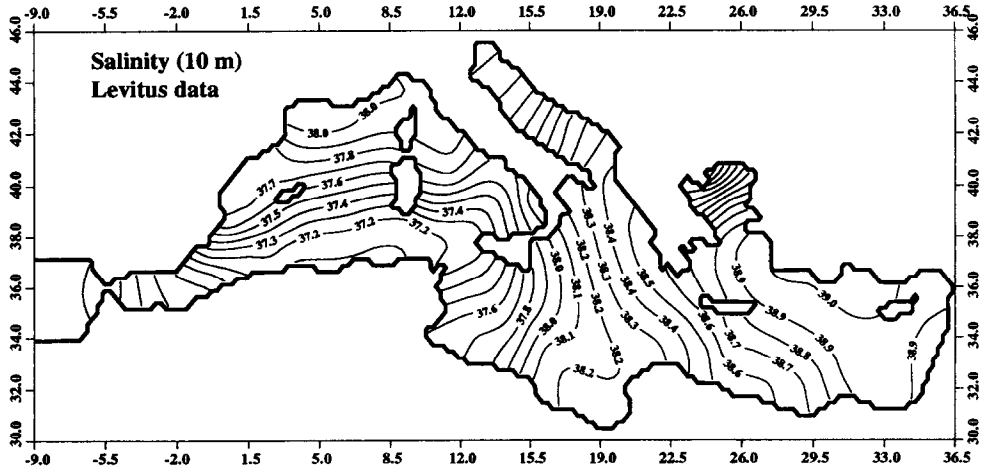

Fig. 1. Climatological salinity field in the Mediterranean surface layer (10-m depth) during winter: contouring of the Levitus (1982) gridded data set.

logistically more accessible (POEM Group, 1992); this provides a unique opportunity for examining the Mediterranean Sea from a climatological point of view.

In this context, we believe that an updated climatological reference, integrating recent CTD data in addition to the bottle data used by the above-mentioned authors, would greatly improve our perception of the dominant processes and forcing mechanisms. Moreover, the digitalized version of the physical fields (taking the shape of three-dimensional gridded data sets) could be easily handled as initial conditions for primitive equation models. The latter point is of particular importance since the renewal timescale associated with the thermohaline circulation is estimated at about 100 years (Hopkins, 1985); it is thus mandatory to position the model initial state as close as possible to the actual climatology, compressing the spin-up time of the numerical process and avoiding possible drift towards unrealistic solutions.

The aim of the seasonal analyses is not to provide a thorough description of the annual cycle, but instead to reproduce four (seasonal) realizations of the climatology. A fully developed annual cycle would necessitate the resolution of the monthly scale, and it will be shown that our data set is not dense enough for that.

In this paper, we shall only describe the scientific framework set up to construct a new climatology, with emphasis on the most significant results obtained from it. The collection of charts and numerical fields, i.e. the atlas itself prepared for general distribution amongst the scientific community (Brasseur *et al.*, 1994), should be considered as a companion document to this paper.

The hierarchy of tasks forming our study is organized as follows. First, an inventory of the original hydrographic information available on the Mediterranean Sea has been undertaken. Our strategy is to gather as many *in situ* data as possible in a unique historical file system (hereafter referred to as the MED2 data set). For that purpose, we have considered both existing NODC data bases and data sets stored at regional institutions. Some aspects of the MED2 data set are addressed in Section 2. In Section 3, we describe a variational inverse methodology developed to calculate the gridded fields from the MED2 data. Indeed, it is obvious that different analysis procedures may lead to different reconstructed climatologies; our preference for the variational method therefore needs some explanation and justification. Finally, in Section 4, the temperature and salinity analyses are examined, with particular attention to the seasonal signal affecting the system. In addition to the classic T/S distributions, the numerical fields allow the derivation of diagnostic products such as geostrophic currents, Brünt–Väisälä frequency and potential vorticity. Some of these properties will be discussed in the paper as well.

In a forthcoming paper, the dynamic adjustment of the circulation to the climatology will be studied in detail with a three-dimensional, free surface, primitive equation model operated in diagnostic/robust mode.

2 THE MED2 HISTORICAL DATA SET

2.1 *Data sources*

There is no doubt that the quality of the analysis results will depend strongly on the quantity of *in situ* measurements. In spite of the numerous surveys and observing programs carried out in the Mediterranean, no exhaustive historical data bank has been compiled in a systematic way. However, two major files containing a substantial part of the experimental

work at sea are readily available: the French BNDO file (Bureau National des Données Océaniques, Brest, France) containing hydrographic casts only for the Mediterranean region, and the U.S. NODC file (National Oceanographic Data Center, Washington, U.S.A.) which is a subset of a world ocean data bank. Thus, our first objective was to merge these two historical files into a single set and to augment it with additional sources released by regional centres.

The BNDO data set consists of about 17,000 vertical profiles (mainly bottle data) taken in the eastern and western basin, the Black Sea and the Atlantic region adjacent to the Strait of Gibraltar. The measurements have been collected since 1911, but the data set is mainly representative of the period 1945–1978. The data point distribution is highly inhomogeneous in space and time. In the western basin, a lot of stations are located in the Gulf of Lions during February, as a consequence of the survey of deep water formation. However, the average density of observations is rather weak during autumn and winter, especially in the eastern basin (Brasseur *et al.*, 1994).

In the BNDO file, the temperature and salinity measurements are given at original sampling depths; however in our version of the NODC file, which contains more than 20,000 profiles representative of the eastern and western Mediterranean basins, the values are interpolated to standard levels. As explained later, this difference in the vertical sampling creates some problems for detecting duplicated records during the merging phase. The coverage of the eastern basin, as well as the southern part of the western basin along the Algerian coast, is much better from the U.S. NODC than from the BNDO data file. Even if overlap exists, the two spatial and temporal samplings are quite different; therefore, one can expect a better representation of the hydrology in a merged version of the two original files.

In addition to these major sources, another data set of about 4000 stations, mostly covering the Adriatic Sea, has been made available by IRPEM (Istituto per la Ricerca sulla Pesca Maritima, Ancona, Italy). The main benefit gained from the latter set lies in its capability of providing a refined climatology over the Adriatic region. Since it has been constituted quite recently (most stations are posterior to 1980), it also contains more accurate data than the previous ones.

Other regional sets, such as the POEM hydrographic data (POEM Group, 1992), have been identified as potential candidates for upgrading MED2. The preparation of these data (flagging, quality checking, formatting and related tasks) is under way, and their final merging with MED2 will be achieved under the leadership of the European MAST programme.

2.2 *Data reduction*

The MED2 historical data set is the result of the merging of the three above-mentioned sources, which had been quality-controlled individually before archival. Although various chemical and biological parameters are sometimes reported in the station records, we have decided to retain the temperature and salinity measurements only, since climatological analyses of parameters other than T/S is often awkward. This is the case for dissolved oxygen observations, which are typically five times less frequent than the T/S data.

One of the most delicate tasks has been the identification of duplicated stations: indeed, a large quantity of hydrographic data had been sent to both centres for final banking. Depending on the protocols used for data representation, the observed values are stored at the original sampling depth (BNDO) or at standard depths (NODC). In the latter case,

interpolation and averaging procedures have been used which are often poorly documented. Thus, the projection of the original data on standard levels might have modified the profiles in an unpredictable way, and the automatic rejection of a duplicate can only be decided on the basis of the header record information. Almost all headers contain the date and position of the stations; however, the precise time of the cast is sometimes omitted in the BNDO or NODC files. Therefore, some conflict may arise if anchored stations include several casts during the same day.

This problem has been encountered at several locations for which even a manual comparison between two casts remains misleading. In order to eliminate any doubt, we decided to keep one version only of such ambiguous stations. After completing the redundancy check, the merged MED2 data set still contained 34,195 hydrographic casts. Nearly 25% of the U.S. NODC data (or 11,000 profiles) were found duplicated at the BNDO, the new profiles being located mostly in the eastern basin.

As already quoted, one of the main motivations of this study consists in the detection and quantification of the seasonal variability in the water masses. In order to accelerate the processing of the observations, the stations were then grouped into 12 climatological files, each of them containing the data relevant to one particular month of the seasonal cycle (whatever the year of the measurement between 1900 and 1986). Then, the seasons are conventionally defined as follows: winter, January + February + March; spring, April + May + June; summer, July + August + September; autumn, October + November + December. In the rest of the paper, we shall mainly concentrate on the winter and summer seasons, although the four periods have been analysed with the same procedure (Brasseur *et al.*, 1994).

2.3 *Data distribution*

The location of the MED2 stations is shown in Fig. 2 for the winter and summer periods. Although more than 6000 profiles are available to describe one single season, the data distribution is fairly inhomogeneous in space. As a rule, more data are found in the western basin than in the eastern one. Some regional seas have been exposed to more intense surveys than others. For instance, the coverage of the Adriatic and the Gulf of Lions is extremely dense, whereas the Levantine basin and the Tunisian shelf suffer from a severe lack of data. In our opinion, this unequal distribution in MED2 rather results from a lack of experiments carried out at sea than from an incomplete inventory of existing data in the southern regions.

The spatial distribution of the data in the monthly sets is quite similar to the seasonal sets, but of course the scarcity of the stations is even more pronounced. As a corollary, error estimates on monthly analyses will often exceed the limit required for legitimate interpretation.

The time distribution of the data displays some trends as well, certain months being sampled more intensely than others (Fig. 3). This is probably related to the tendency to intensely investigate specific processes; for instance, the large number of data in February can be explained as the consequence of the many surveys organized for years in the Gulf of Lions to track the deep water formation.

It is well known that the Mediterranean undergoes not only a seasonal cycle but also interannual variabilities (e.g. Hecht *et al.*, 1985) that may affect the heat and buoyancy fluxes, the upper layer properties (Garrett *et al.*, 1993) and also the deep water masses

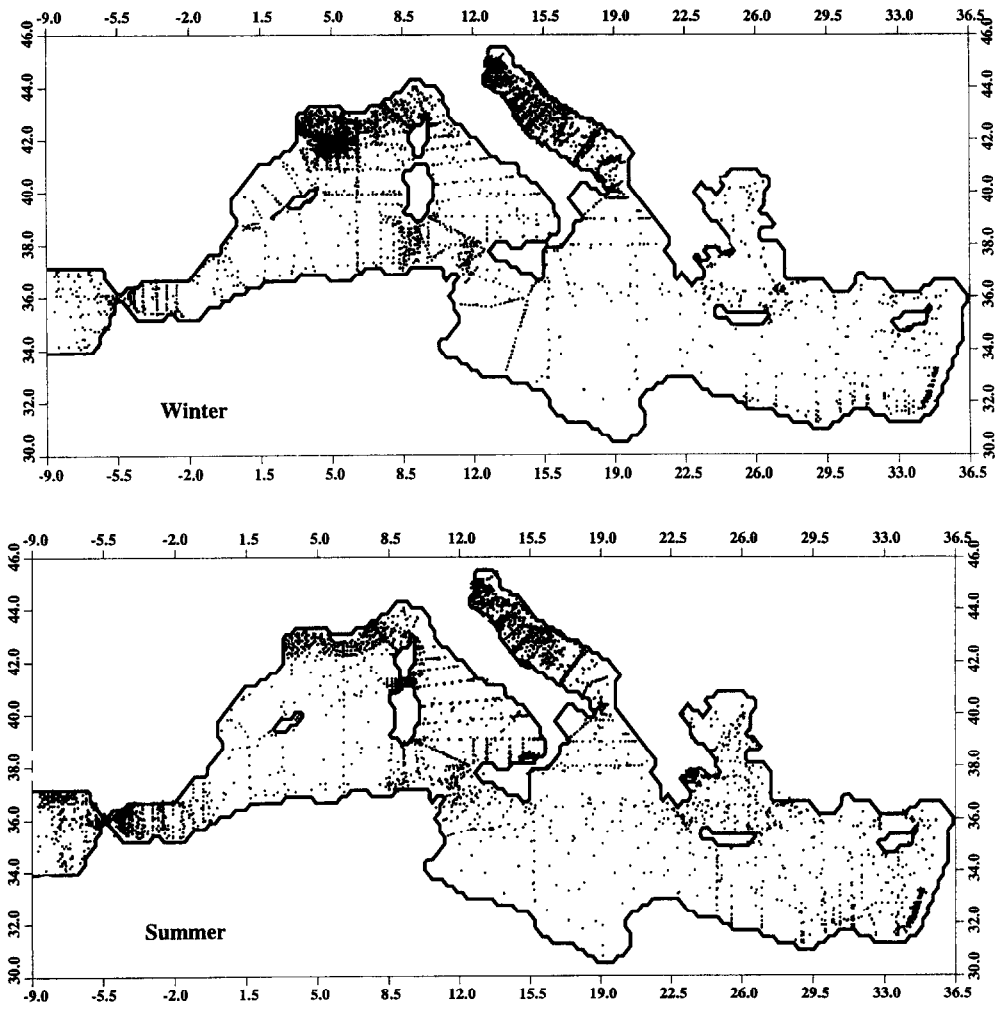

Fig. 2. Location of hydrological casts incorporated into MED2 for the winter and the summer seasons; the data base contains, respectively, 6816 and 7467 stations.

(Bethoux and Tailliez, 1994). The volume of data gathered within MED2 will not allow resolution of these interannual variabilities, at least on the scale of the global basins. In the same way, the temperature drift observed in the deep layer by Bethoux and Tailliez (1994) and Rohling and Bryden (1992), which is actually small compared to the spatial variations, will be ignored in our climatological analyses. Therefore, the data will be globally analysed, without any discrimination between the years of acquisition. In the near future, additional data will complement our MED2 historical records, offering a more significant description of the period 1980–1990 and the possibility of longer-timescale variability studies.

Figure 4 illustrates the distribution of the MED2 data from 1900 to 1986: more than 80% of the observations are representative of the period from 1945 to 1980, with an almost constant distribution along this interval. Thus, it is assumed that decadal variabilities will be filtered out reasonably well. One could expect that a future upgrade of MED2 with data

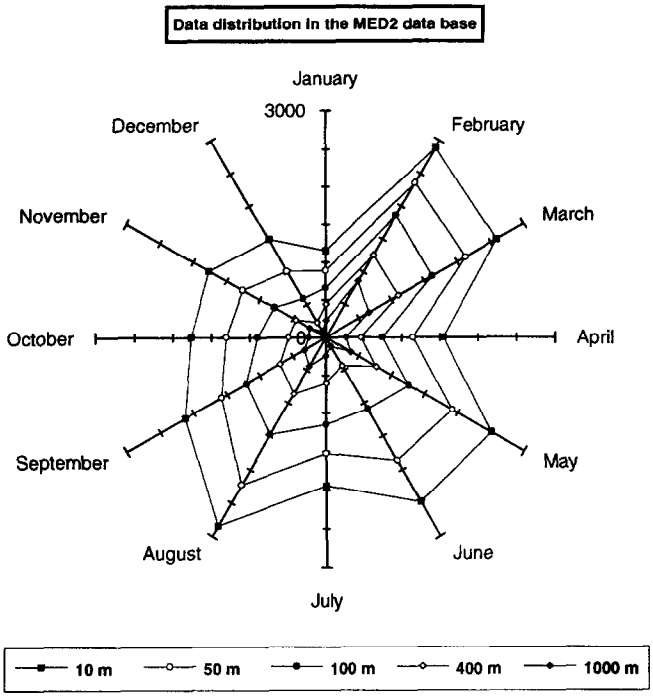

Fig. 3. Monthly distribution of the MED2 data through the annual cycle; the number of casts ranges from about 1200 in January to nearly 3000 in February and August.

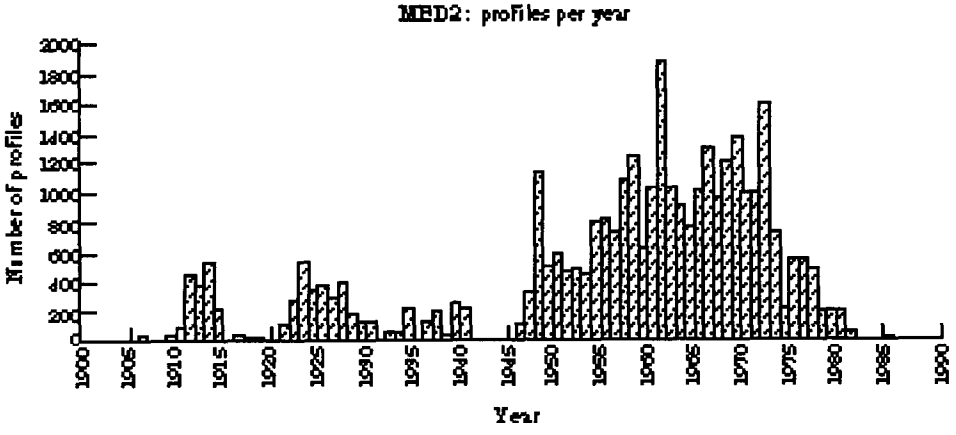

Fig. 4. Historical distribution of the MED2 data between 1900 and 1986; more than 80% of the measurements are representative of the period 1945–1980.

collected during the 1980s (for instance, integrating XBT measurements) could drastically improve the capability to estimate a possible climate drift.

2.4 *Data statistics*

Before discussion of the reconstruction procedure in detail, several statistical parameters can be extracted from the monthly (or seasonal) data collections. Indeed, estimates of the noise and correlation scales are required for statistical interpolations and to attach error bars to the analyses. Although the statistics may vary from one region to another, it is customary to invoke assumptions like statistical isotropy and homogeneity on the behaviour of the fields (Gandin, 1969). These simplifications are justified by the need to get enough observational samples to compute averaged quantities. Therefore, the only distinction we shall investigate is the dependence of the noise and correlation scales on depth, assuming merely horizontal isotropy and homogeneity.

Roughly speaking, the noise (or, equivalently, the standard deviation of observational errors) can be interpreted as a root mean-square average of the difference between the data and their mean value within 30×30 km boxes, i.e. within regions covered by two or three Rossby radii of deformation. It includes several contributions: sub-mesoscale and mesoscale variability, interannual changes, instrumental errors, and others. However, the relative scarcity of the data in some regions precludes the direct computation of an algebraic average from the raw measurements. This is why more reliable procedures, based on the concept of cross-validation (e.g. Wahba, 1990), have been developed to directly estimate the noise from the observations. The philosophy of cross-validation consists in leaving aside part of the original data when performing the analysis, and to use those data left out to measure the misfits between the filtered and unfiltered fields. After repeating the process for many different partitions of the data set, one gets a sound statistical estimate of the noise in the observations. The details of this procedure are fully described in Brankart and Brasseur (1996).

In the examination of oceanographic data, it is often found that the amplitude of the standard deviation is maximal near the surface and abruptly decreases with depth, as illustrated in Fig. 5. Vertical bars represent 90% confidence intervals in the estimates, which quantifies the reliability of the curves. Thus, the time sampling is sufficient to yield reliable global statistics, while the regional sub-division of the data set would result in unacceptable confidence statistics. As discussed in Section 4, seasonal changes in the statistics do not reflect time incoherence of the data set but, instead, the modifications of the stability conditions in the upper layer. Because instrumental errors are almost depth-independent, the natural variability of the physical system (which is mainly related to air–sea interactions) is responsible for the high noise level observed near the surface. The curves on Fig. 5, which correspond to the four seasonal sets, indicate that the temperature data in the upper layer are about four times more noisy during summer and autumn than during winter.

Using the cross-validation procedure, the autocorrelation of the fields is estimated within each of the Mediterranean water masses, i.e. Atlantic Water, Levantine Intermediate Water and Deep Water. It is found that our estimated correlation scales are almost independent of the basins (this point has been tested in calculations with all data together, or in separate calculations for the eastern and western sectors) and do not significantly differ from one water mass to another. As in Thiebaux (1975), an analytical expression is adjusted to the experimental covariances calculated from all pairs of observations. The mathematical

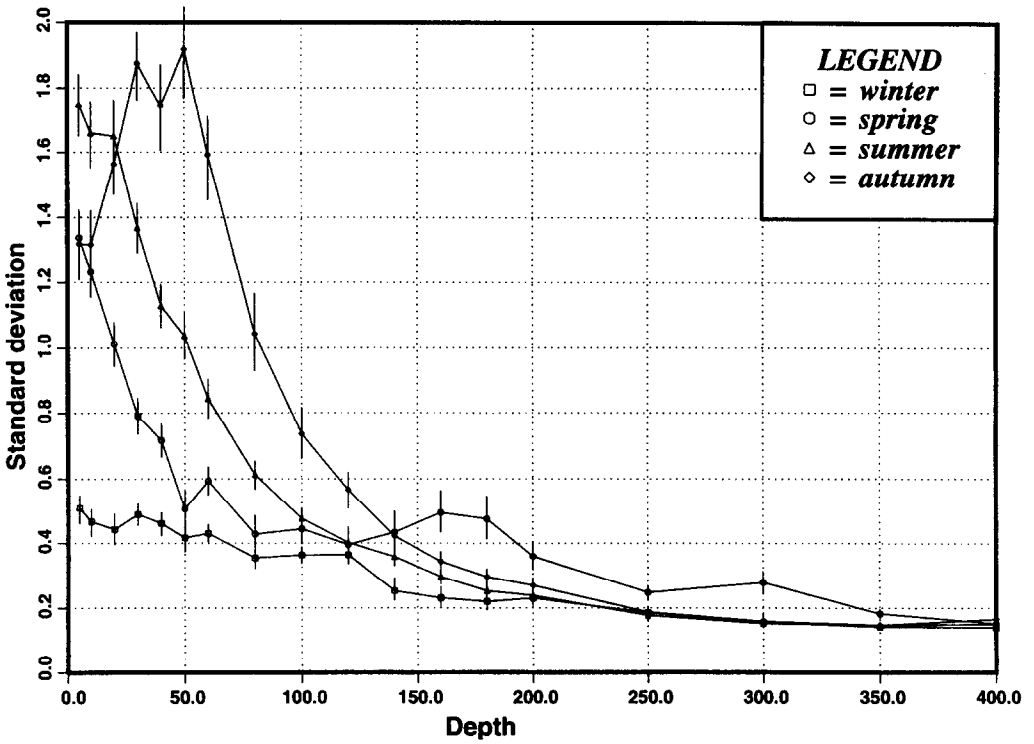

Fig. 5. Standard deviation of observational errors in temperature (°C), calculated as a function of depth; the four curves correspond to the seasonal MED2 data sets. Vertical bars depict the 90%-confidence interval in the estimates.

structure of our correlation function reads

$$K(r) = \left(\frac{r}{L}\right) K_1\left(\frac{r}{L}\right) \tag{1}$$

where r is the Euclidian distance, L is the parameter controlling the decay of the modelled correlations and $K_1(r)$ is the modified Bessel function of order 1 (Fig. 6). This particular choice for the correlation model results from the mathematical structure of the variational method discussed in Section 3. The value of 80 km for the length scale in (1) corresponds to the best fit to the correlations observed in Fig. 6. Technical aspects of these calculations, including the application of the cross-validation technique, are reported in Brankart and Brasseur (1996).

One should point out that the noise and spatial scales estimated from the MED2 data directly depend on the way the observations have been sorted; in other words, the merging of the data into seasonal sets itelf determines the scales of what we define as the seasonal circulation. This is a consequence of the spectral distribution of the physical processes, not a deficiency due to the limited size of the data base. Thus, expression (1) and the corresponding estimates of L indicate that gyres with a radius of about 100 km are expected to produce some residual effects on the general circulation. This conclusion confirms our initial objection to consider the Levitus analyses, which exhibit much larger patterns (Fig. 1), as representative of the seasonal circulation in the Mediterranean.

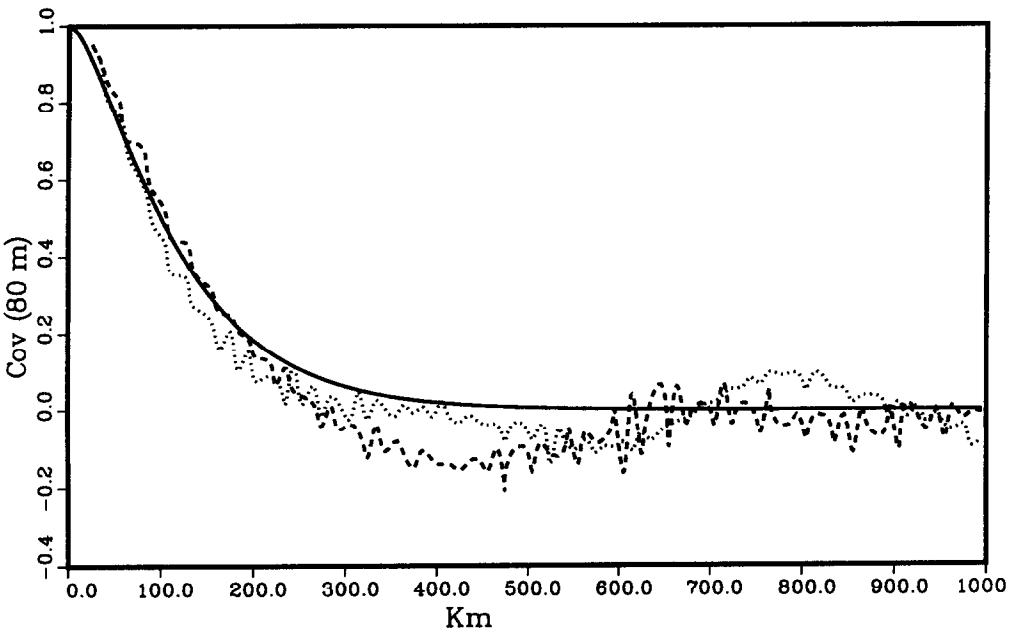

Fig. 6. Correlation function as estimated from the MED2 data in the upper layer (80-m depth): the dotted (dashed) line represents direct calculations from experimental temperature (salinity) values and the continuous line is the model correlation (1) with parameter L adjusted to 80 km.

3 THE VARIATIONAL INVERSE METHOD AS OBJECTIVE ANALYSIS

The next step consists of reconstructing continuous temperature and salinity fields representative of the mean climatological state of the sea. The "redistribution" or "gridding" of values from irregular networks (as in Fig. 2) to regular grids is sometimes justified by the need to provide initial or boundary conditions to numerical models (which are generally discretized on regular finite difference grids) or simply to present a comprehensive picture of the data for further examination and interpretation.

3.1 *Optimal and sub-optimal methods*

In order to eliminate the noise associated with the measurements, the interpolation on the regular grid must be achieved concurrently with an appropriate filtering of the observed values. Methods known as objective analysis (OA) have been widely used in meteorology and oceanography (e.g. Gandin, 1969; Bretherton *et al.*, 1976) to solve this two-fold interpolation/filtering problem. The standard OA scheme relies on a quite simple statistical result: the Gauss–Markov theorem. The "best" analysis, defined as the estimate which provides the minimum expected error, can be obtained by solving a simple linear algebraic problem. The only prior knowledge required by this process concerns the covariance of the unknown field and the standard deviation of observational errors.

Although objective analysis has become very popular within the oceanographic community, the straightforward application of the statistical scheme is ineffective in analysing huge historical sets containing thousands of data points. Indeed, the size of the

linear system to be inverted is equal to the number of observations in the set. Of course, it is often possible to fragment the data into subsets, taking into account the very weak correlation between points separated by more than two or three decorrelation distances. Another possibility consists in grouping the data into "super-observations" representative of the averaged data within specified boxes (Robinson and Leslie, 1985).

A variety of other devices can be invoked to reduce the size of the algebraic problem; however, at the same time, they lead to degradations of the original scheme because several arbitrary decisions must be taken. That is, the procedure is not "optimal" any more. Let us mention that iterative procedures such as those used by Levitus (1982) also necessitate subjective choices.

In addition, difficulties may arise from the complicated nature of the oceanic domain, which is the support of the analyses. As a consequence of the statistical assumptions on the behaviour of the fields, the correlations are most often estimated as a function of the Euclidian distance between the points involved. If two oceanic regions are separated by land (as, for instance, between the Adriatic and the Tyrrhenian Sea), observations in either region should be decorrelated more acutely than in the absence of land. This is primarily true for temperature and salinity, since the presence of land creates an obstacle to their propagation in the sea. Again, the algebraic objective scheme (as it is applied in the current practice) needs some modification to take this effect into consideration.

Instead of performing these degradations, some authors (e.g. Lorenc, 1986) recommend the application of procedures in which human intervention is reduced to a strict minimum. In this perspective, we have developed a variational method that is initially inspired by a personal intuition rather than by a purely statistical principle. In spite of this apparently subjective approach, we shall demonstrate a very close analogy between the classical OA scheme and our intuitive method. The concept of variational analysis has been introduced by Sasaki (1970) and then extended by Wahba and Wendelberger (1980) in the context of meteorological applications.

3.2 *The variational analysis method*

The basic idea of the variational analysis is to determine a distribution which, although sufficiently close to the data, exhibits small spatial variations only. In other words, the target of the analysis (say, ϕ) is defined as the smoothest field that respects the consistency with the observed values over the domain of interest. In this paper, we shall just recall the method, which is extensively described in Brasseur (1991) or Brasseur and Haus (1991).

Expressed in mathematical terms, the analysis is obtained as the minimum of a variational principle (in the two-dimensional, horizontal space):

$$J[\phi] = \int_{\Omega} \{S[\phi] + D[\phi]\} \mathrm{d}\Omega \tag{2}$$

with

$$S[\phi] = \left(\frac{\partial^2 \phi}{\partial x^2}\right)^2 + \left(\frac{\partial^2 \phi}{\partial y^2}\right)^2 + 2\left(\frac{\partial^2 \phi}{\partial x \partial y}\right)^2 + \alpha_1 \left(\frac{\partial \phi}{\partial x}\right)^2 + \alpha_1 \left(\frac{\partial \phi}{\partial y}\right)^2 + \alpha_0 \phi^2$$

and

$$D[\phi] = \mu \sum_{i=1}^{N} [\phi(x, y) - d_i]^2 \delta(x - x_i)\delta(y - y_i)$$

The integral extends over Ω, i.e. the Mediterranean Sea domain. The first contribution in the variational principle $S[\phi]$ is a measure of the roughness of the target field. It is easy to prove that this operator is invariant with respect to any rotation of the reference frame. The coefficients α_0 and α_1 fix the weights of the lower derivatives in the smoothing operator. The second term, $D[\phi]$, represents the distance between the data d_i observed at location (x_i, y_i) and the target field; its weight μ is determined according to the confidence in the data. In principle, the value of the weight could be adjusted to every observation individually, but in practice it is impossible to decide whether one observation is more reliable than another.

The variational analysis is also referred to as a spline interpolation method. In practice, all observations available at a given depth are selected from the MED2 data set to perform the minimization in a horizontal plane. The reconstruction of a three-dimensional scalar field is then obtained as a superposition of several analyses corresponding to different depths. This reduction of the size of the problem is made possible because the data profiles describe the vertical structure of the sea reasonably well and do not produce hydrostatic instabilities. One could certainly proceed in a slightly different way. For instance, gridding the data on isopycnal surfaces might work equally well and would make the smoothing criterion even more meaningful.

Different versions of variational analysis are described in the literature (e.g. Wahba, 1990). McIntosh (1990) defines two different measures of field smoothness: norm splines, which take into account the field amplitude and curvature; and semi-norm splines, in which only curvature is considered. Although the two versions of splines often lead to similar results, it is worth noting some important differences. When $\alpha_0 \neq 0$, the norm splines necessitate a first-guess field, because the quantities to be analysed must represent departures with respect to some mean reference (otherwise, the averaged amplitude of the field would also be minimized during the process); in practice, we calculate the least-square linear regression of the data, as suggested by Bretherton *et al.* (1976), in order to remove the mean and the spatial trend in the observations. As demonstrated later on, norm splines have the advantage of emulating OA, including error estimates on the results. Conversely, semi-norm splines (i.e. $\alpha_0 = 0$) do not require a first guess since the field amplitude is not penalized; in that case, the quantity which is analysed might be the "total" field. The statistical interpretation of semi-norm splines however is less obvious.

To examine the qualitative behaviour of our formulation in a more comprehensive way, it is instructive to consider the Euler–Lagrange equation, which can be derived from the variation of (2):

$$\Delta^2\phi - \alpha_1 \Delta\phi + \alpha_0 \phi = \mu \sum_{i=1}^{N} (\phi - d_i)\delta(x - x_i)\delta(y - y_i) \tag{3}$$

For the moment, let us assume that the weights on the lower derivatives are small enough to keep the left-hand-side dominated by the biharmonic term. The partial differential equation (3) is similar to the mathematical model describing the deflection of thin plates subject to transverse loading (Zienkiewicz, 1977): each data point plays the role of a pinpoint load that locally "attracts" the target field toward the observation, imposing the global shape of the solution. When $\alpha_1 \neq 0$, the solutions of the variational problem are

identified as splines-in-tension (Franke, 1985), because their behaviour is similar to that of thin plates constrained by lateral tension.

This mechanical analogy may be exploited in several ways. For instance, it supplies a convenient guide for intuitively determining the approximate behaviour of the variational procedure and the qualitative aspect of the results. It is well known that the mechanical deflection of a thin plate must be achieved without local discontinuities or "breaks", indicating that the solution must be continuously derivable. By analogy, the variational analysis method will remove sharp gradients, prevent the representation of oceanic fronts and moderate the effect of spurious oscillations in the data.

Another advantage of the "thin plate" model is that numerical techniques developed in structural engineering can be naturally adapted to compute the minimum of variational principles like (2). Compared to the work of several other authors (e.g. Wahba and Wendelberger, 1980; McIntosh, 1990), the originality of our formulation lies in the minimization of the field curvature over the real domain of interest only (integral over Ω in (2)). For atmospheric applications, the analysis domain can be considered as unbounded in the horizontal direction; however, the situation of the ocean is much different since its extension is most often limited by coasts. It is thus impossible to obtain rigorous analytical solutions to the minimization problem over Ω, but the finite-element method may produce a very convenient and flexible tool for doing this. The concept of finite elements consists in dividing the global domain into smaller sub-domains in which the solution is parameterized as

$$\phi(x, y) = \sum_{k=1}^{M} q_k s_k(x, y) \tag{4}$$

where $s_k(x,y)$ are known shape functions (like polynomials) defined on each element and q_k are unknown coefficients. Technical details on the finite-element procedure are given in Brasseur (1994).

The finite-element discretization of the Mediterranean domain used for the reconstruction of the climatology is illustrated in Fig. 7. The size of the triangles is chosen so as to authorize the numerical representation of the gyres representative of the general circulation, following the correlation length scales indicated in Fig. 6. Let us mention that the nodes of the grid are distributed as regularly as possible. In particular, there is no constraint related to the position of the observations; all data are analysed at their exact location as stipulated in (2), without any prior re-gridding or whatever. The minimization problem can now be expressed in terms of the new degrees of freedom q_k. After substituting (4) into (2), one gets a linear algebraic system:

$$\mathbf{Kq} = \mathbf{g} \tag{5}$$

in which $\mathbf{q}$ is the vector of unknown coefficients q_k, $\mathbf{g}$ is a vector containing the contribution of the data d_i and $\mathbf{K}$ is the classical "stiffness" matrix constructed from the integration of the shape functions $s_k(x,y)$. The size of the numerical problem associated with (5) will depend on the number of coefficients q_k used for the finite-element discretization. Compared to objective analysis, the computational burden is thus independent of the volume of the data set: this peculiarity will be in favour of the variational method when huge historical data sets have to be analysed.

The choice of a suitable basis of shape functions must be guided by the mathematical

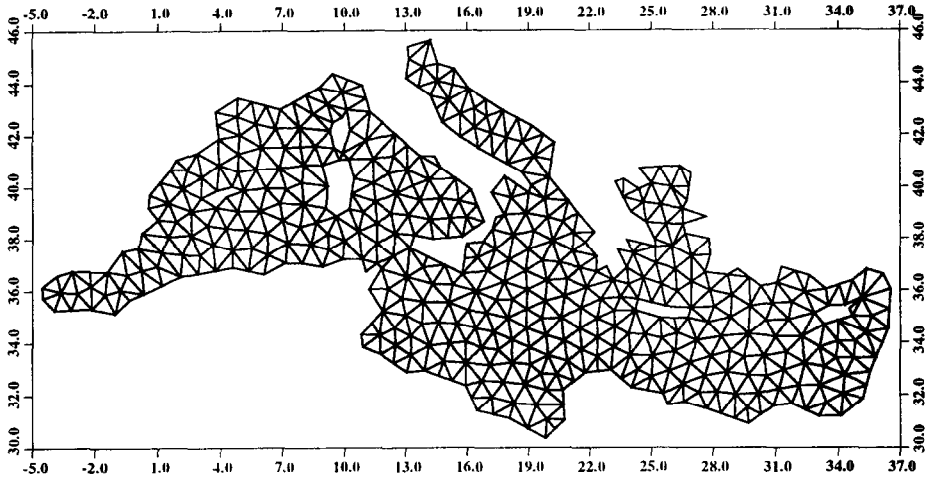

Fig. 7. Finite-element discretization of the Mediterranean domain into 770 triangles (corresponding to a total of 2786 degrees of freedom).

nature of the partial-differential problem at stake. As demonstrated in Wahba and Wendelberger (1980), the δ-functions appearing in (2) require the presence of, at least, second-order derivatives in the smoothing operator. Thus, the functional space considered here must belong to the family of the $H^2(\Omega)$ Sobolev spaces. In the finite-element context, one can show that a finite-element basis V_h consisting of piecewise polynomials belongs to $H^2(\Omega)$ if, and only if, the functions of V_h and their first derivatives are continuous (Johnson, 1990). This mathematical property was already quoted in the discussion of the thin-plate models.

Given this mathematical exigency, we have selected the finite element introduced by Veubeke (1974) to solve the numerical problem of plate bending. Roughly speaking, this element consists of a fourth-order polynomial development similar to (4), in which the coefficients q_k are subject to constraints expressing the $H^2(\Omega)$-property of the global solution. Different numerical tests have demonstrated its efficiency and accuracy for solving the variational analysis problem (2). One of these tests will be examined later.

After inversion of (5), it is straightforward to extract the values of the solution (4) at arbitrary points because the shape functions have been determined *a priori*. For practical reasons, the reconstructed data are usually extracted at the nodes of a regular grid, but another choice could be made as well. One should make clear that the latter stage doesn't introduce additional smoothing of the original data since the final gridding is nothing but a discrete representation of the continuous function (4).

Let us also mention that statistical estimates of the variance of the solution can be computed, following the same approach as in OA:

$$\mathbf{V} = \overline{(\mathbf{q} - \hat{\mathbf{q}})(\mathbf{q} - \hat{\mathbf{q}})^T} \tag{6}$$

where $\hat{\mathbf{q}}$ represents the exact solution. After substitution of $\mathbf{q} = \mathbf{K}^{-1}\,\mathbf{g}(\mathbf{d})$ in (6) and some manipulations, the diagonal terms of this matrix provide error bars on the solution in terms of the finite-element degrees of freedom.

3.3 *Comparison between objective and variational analysis*

At first glance, the variational method could appear as an intuitive procedure that suffers from a lack of rational background. However, this impression can be disputed due to the existence of a mathematical equivalence between splines and statistical OA. This equivalence has been demonstrated by McIntosh (1990), both theoretically and by comparing the two methods in academic cases. Here, we shall reinforce this evidence using real data collected in the Mediterranean basin.

Let us first introduce a characteristic length scale L in the variational principle (2), and convert the dimensional weights and into non-dimensional quantities, as

$$\beta_0 = L^4\alpha_0 \quad \text{and} \quad \beta_1 = L^2\alpha_1 \tag{7}$$

The various terms in the smoothing operator are of comparable magnitude for the choice of $\beta_0 \sim O(1)$ and $\beta_1 \sim O(1)$. Following the notations of McIntosh (1990), the solution of the variational problem (2) can be expressed as

$$\phi(\mathbf{x}) = \sum_{i=1}^{N} c_i \eta_i(\mathbf{x}) \tag{8}$$

with

$$\eta_i(\mathbf{x}) = K(\mathbf{x}, \mathbf{x}_i)$$

The two-point function $K(\mathbf{x},\mathbf{x}_i)$ is the reproducing kernel associated with the Hilbert space of our problem ($\mathbf{x}$ designates any point of the domain Ω, while $\mathbf{x}_i$ is an observation point), and verifies the partial differential equation:

$$\Delta_x^2 K(\mathbf{x}, \mathbf{y}) - \frac{\beta_1}{L^2}\Delta_x K(\mathbf{x}, \mathbf{y}) + \frac{\beta_0}{L^4} K(\mathbf{x}, \mathbf{y}) = \delta(\mathbf{x} - \mathbf{y}) \tag{9}$$

The coefficients c_i are determined as follows:

$$\{c_i\} = \mathbf{M}^{-1}\{d_j\} \quad \text{and} \quad [\mathbf{M}]_{ij} = \frac{1}{\mu}\delta_{ij} + K(\mathbf{x}_i, \mathbf{x}_j) \tag{10}$$

Assuming that the domain Ω extends toward infinity, the exact solution of (9) is a function of the distance between $\mathbf{x}$ and $\mathbf{y}$ only, and can be calculated analytically for particular choices of β_0 and β_1 (McIntosh, 1990); for instance, taking $\beta_0 = 1$ and $\beta_1 = 2$, the reproducing kernel is exactly given by $L^2K(r)/4\pi$, where $K(r)$ is given by equation (1).

The comparison between the exact solution (8)–(10) and the classical OA scheme (e.g. Bretherton *et al.*, 1976) indicates that the two methods are strictly equivalent if the covariance of the process is taken as

$$c(r) = \sigma^2 K(r) \tag{11}$$

and if the variance of observational errors ε^2 is related to the weight on the data by

$$\varepsilon^2 = \frac{\sigma^2 4\pi}{\mu L^2} \tag{12}$$

According to (11), the variance of the signal is denoted by σ^2. In practice, OA solutions are computed at a given point as the linear combination of covariance functions (8) after

resolving the linear system (10). Conversely, the minimization of the variational principle is obtained from the numerical solution of the finite-element system (5).

This mathematical equivalence has two main consequences. First, it provides a statistical justification (and interpretation) of the variational analysis method. Secondly, it indicates how the parameters in the variational principle (i.e. essentially the length scale L and the weight on the data μ) can be related to the statistics of the data set. For instance, the determination of the weights on the data amounts to the evaluation of statistical properties from the measurements, and there is not more subjectivity in the calibration of the variational method than in the choice of observational errors and covariance function to perform OA. In the rest of the paper, we shall thus adjust these parameters according to the statistical properties illustrated by Figs 5 and 6.

Of course, the strict equivalence will be slightly modified with respect to (11) by the existence of coasts at finite distance: the real oceanic domain (as it has been discretized by the finite-element mesh, see Fig. 7) will introduce some adjustment of the kernel in the vicinity of coasts and other boundaries. In such regions anyway, it is recognized that traditional OA often leads to unphysical results (Robinson *et al.*, 1991; Özsoy and Güngör, 1994).

One can expect that the side effects will be weak, except when the data are concentrated in the coastal zone. To explain this, and to check the correct implementation of the finite-element scheme, a series of comparative analyses has been performed by both the statistical OA and the variational inverse methods (Brasseur, 1994). Figure 8 illustrates the reconstruction of the temperature field at 100-m depth during February as obtained from the two methods: a visual examination reveals only marginal differences between the two pictures. In addition to confirming the equivalence of the schemes, this comparison indicates that the finite-element method is properly implemented; it also suggests that the resolution of the mesh on Fig. 7 is sufficient to reproduce the dominant features with an excellent accuracy.

From the data distribution in Fig. 8, it is easy to understand that the effect of boundaries will be small: indeed, only a few stations are located in the coastal zone. By contrast, the data set corresponding to the surface salinity in November has a rather different shape (Fig. 9): in the Adriatic, many stations have been collected along the Italian side, while the Tyrrhenian Sea is almost void of data. This particular station distribution, combined with the strong physical transition between Adriatic and Tyrrhenian water properties, results in the differences observed between the reconstructions shown in Fig. 9. Although variational and objective analyses behave very much alike in most regions, the salinity in the Tyrrhenian Sea exhibits two rather distinct patterns. More precisely, one observes the strong influence of coastal Adriatic data (characterized by very low salinity values) on the Tyrrhenian region when OA is used. The spot of low salinity encountered along the Tyrrhenian coast of Italy (Fig. 9(a)) is in total contradiction with data from other monthly sets, demonstrating the artificial nature of the minimum. This artefact is a direct consequence of the statistical isotropy that has been assumed to run the objective scheme: information contained in the

Fig. 8. Temperature field at 100-m depth during February, as reconstructed from (a) the statistical OA scheme, and (b) the variational inverse method. The parameters of the two methods have been adjusted according to the statistics of the data and the conditions of equivalence discussed in the text; the spatial distribution of the data used for this reconstruction is shown in (c).

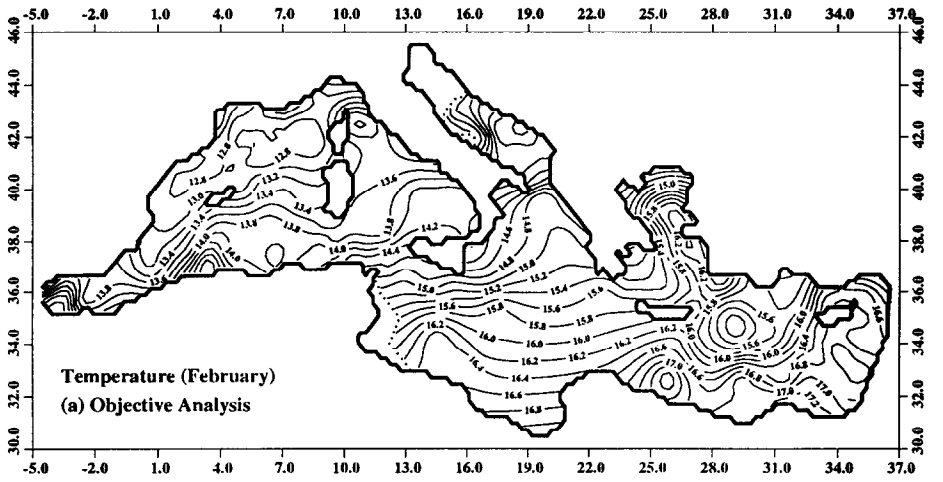
Temperature (February)
(a) Objective Analysis

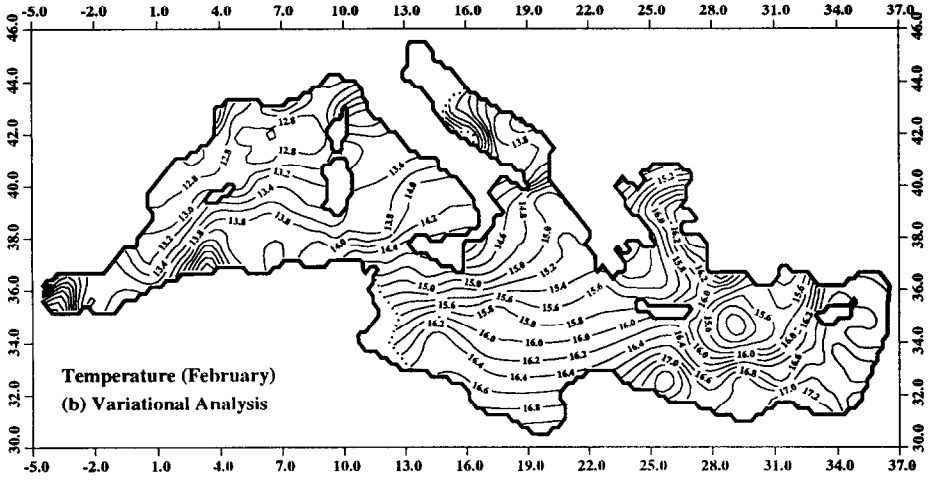
Temperature (February)
(b) Variational Analysis

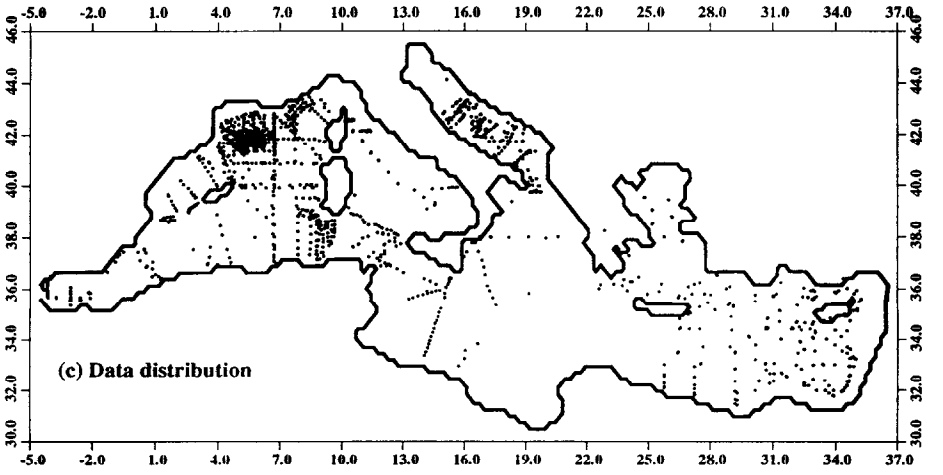
(c) Data distribution

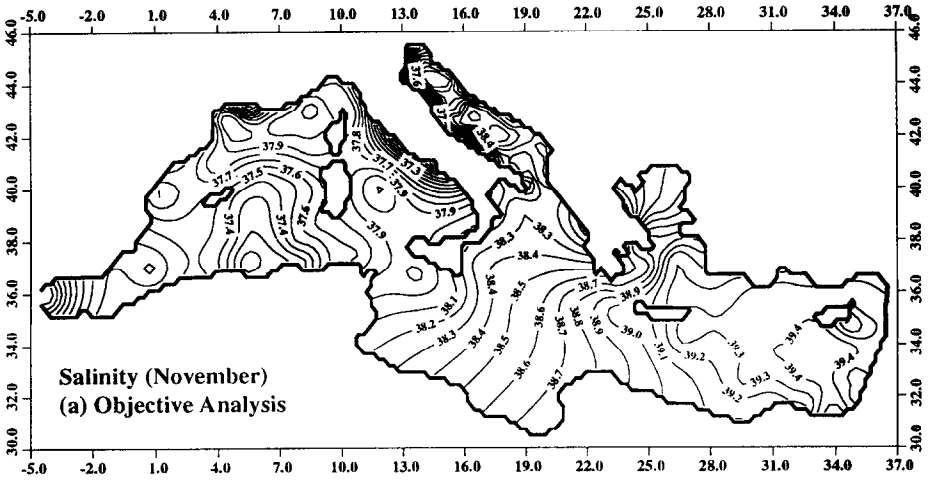
Salinity (November)
(a) Objective Analysis

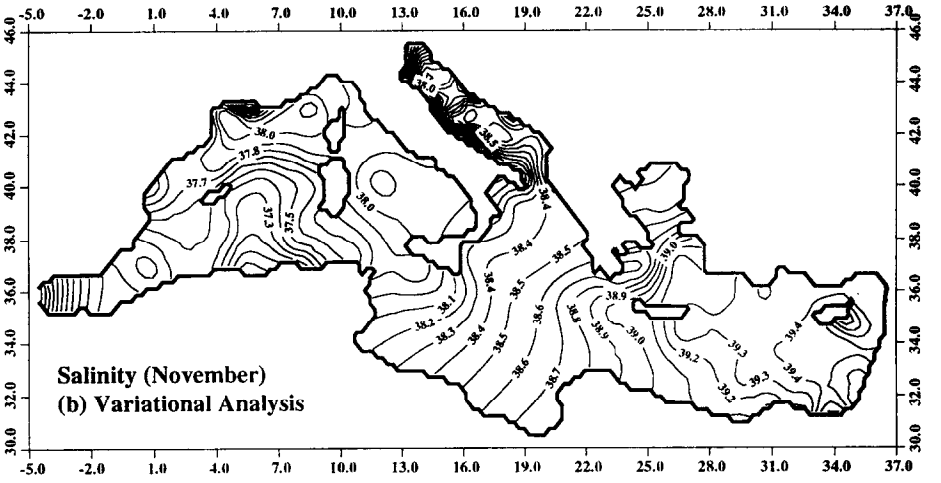
Salinity (November)
(b) Variational Analysis

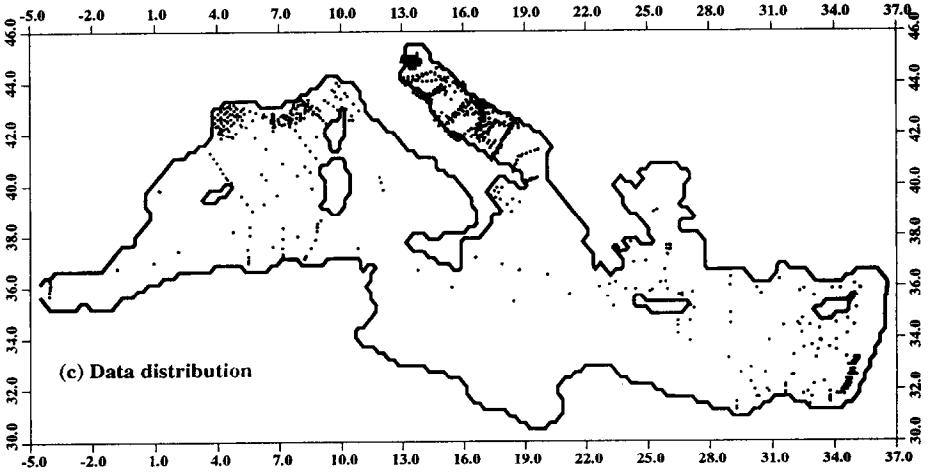
(c) Data distribution

Adriatic data has been propagated "across Italy", over a distance of about two correlation length scales.

Of course, one could certainly take into account the existence of land between sea regions by decreasing the correlation between points separated by land. However, one should still decide in which circumstances such points have to be considered as completely disconnected; this particular treatment could also increase the computer time of the numerical procedure. By contrast, the variational inverse method naturally and progressively induces decorrelations associated with the geometric configuration of the domain. This is because the minimization of the curvature is achieved on the surface corresponding to the real ocean. For instance, the mesh of Fig. 7 is characterized by the absence of finite elements over the Italian land region; therefore, it prevents the propagation of information from Adriatic data into the Tyrrhenian Sea. The variational analysis of Fig. 9 clearly illustrates this mechanism.

The comparisons described above have demonstrated the interest of the variational method as an alternative to the Gandin (1969) objective scheme, at least from an oceanographic point of view. Its advantages in terms of numerical efficiency and computer resources have also determined our preference for the variational analysis. The numerical costs of both methods can be qualitatively estimated on the basis of the equations discussed above, namely equation (5) for variational (finite-element) and (8)–(10) for objective analysis.

The number of algebraic operations necessary to produce a two-dimensional gridded field using OA is approximately given by

$$C^{OA} = k_1 N^3 + k_2 NP \tag{13}$$

where P is the number of grid points ($\sim$4000 in the 0.25° configuration of the Mediterranean). The first contribution, proportional to N^3, corresponds to the computation of "influence coefficients" c_i from equation (10); the second term arises from the linear combinations (8) which must be evaluated at every grid point. Computation costs may be reduced by decreasing the size of the original data set: one possible device is to contruct a new set of "super-observations" by averging the data within small boxes or spheres. The cost of those sub-objective methods behaves according to equation (13), in which the total number of observations N is replaced by the reduced number of super-observations (Robinson and Leslie, 1985).

Another sub-optimal method consists of analysing the data locally, i.e. inverting data located within a sphere of influence around each estimation point. The radius of those spheres is usually set proportional to the correlation length scale, but the data selection can take into account the existence of geographical barriers as well. This is an interesting modification of the original scheme that has several advantages, namely to reduce computing costs and to prevent the non-desired contamination of water properties as noted in Fig. 9(a). One should however remember that the search algorithm needed to fulfil the data selection in the vicinity of each grid point might be as costly as (or even more expensive than) the data inversion itself.

Compared to equation (13), the cost of the variational scheme is evaluated quite differently: equation (5) indicates that the expensive operation is the resolution of a linear

Fig. 9. Like Fig. 8, but for the salinity field at 10-m depth during November.

system, which is basically an $O(M^3)$ algorithm with M being the number of degrees of freedom of the finite-element discretization. As explained in Brasseur (1994) however, it is possible to reduce the cost of this process to $O(M^{2.5})$ using the skyline algorithm to assemble the stiffness matrix (Dhatt and Touzot, 1984). Thus, the equivalent of equation (13) for the variational analysis becomes

$$C^{VAR} = k_3 M^{2.5} + k_4 MP \tag{14}$$

which is independent of the number of observations. Equation (14) evinces the fact that variational analysis is resolved in the "model" space instead of the observational space.

A comparison of the numerical performances of the schemes is illustrated in Fig. 10, in which the CPU time required by variational, objective and sub-objective methods is drawn as a function of the number of observations. In this experiment, the default configuration of the model is that of Fig. 7 using a finite-element mesh of 2786 degrees of freedom; numerical benchmarks have been performed on an IBM RISC/6000 (model 375) workstation.

As expected, the cost of the variational method is nearly independent of the number of observations. While OA competes quite well with the variational scheme for small data sets, algebraic procedures become more expensive as soon as the size of the data set exceeds 400. Even if the increase of the computer time is much slower with sub-optimal methods, the difference between variational and sub-optimal analysis becomes significant for large data sets. For instance, the inversion of a seasonal set containing 6816 data points leads to ~ 58 s for the sub-optimal method and 18 s only for the finite-element scheme. The finite-element resolution of the variational analysis is thus very attractive, especially for the mapping of large collections of historical records.

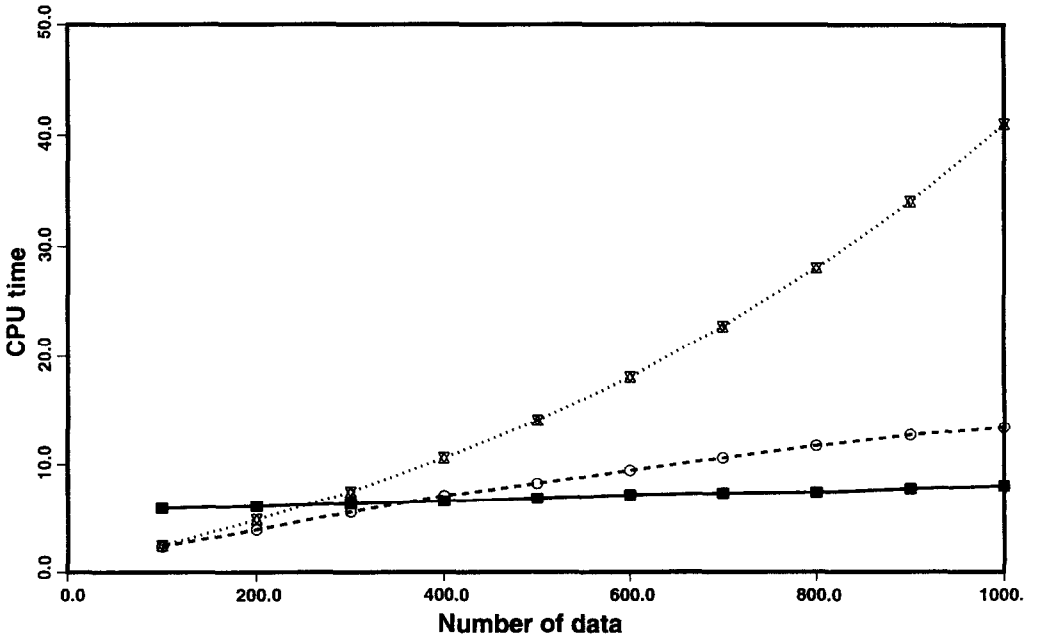

Fig. 10. CPU time (s; benchmark performed on IBM RISC/6000–375 workstation) needed to perform variational (solid line), objective (dotted line) and sub-optimal (dashed line) analysis as a function of the number of observations.

From a methodological point of view, it is interesting to note that the variational framework allows the natural integration of additional constraints to the terms of principle (1) (e.g. Sasaki, 1971; Provost, 1987). As an example, advective constraints have been experienced by Brasseur and Haus (1991) to reconstruct quasi-synoptic situations from sparse data collected during specific surveys. The principal interest in such constraints is to introduce anisotropic correlations resulting from the dominant advective regimes. However, the benefit gained from such constraints has been shown to be negligible in the analysis of climatological situations (Brasseur, 1994), so this option will therefore be ignored in the following.

4 RESULTS: CLIMATOLOGICAL FIELDS IN THE MEDITERRANEAN

Reviews and synthetic descriptions of the general circulation in the Mediterranean Sea can be found in Hopkins (1985), Millot (1987), Malanotte-Rizzoli and Hecht (1988), La Violette (1990) or POEM Group (1992). Since a detailed discussion of the results largely extends beyond the limits of this single paper, we shall only examine some of the most typical products of the variational analysis applied to the MED2 data sets. Selected sections in the summer and winter climatological distributions will be given special attention. An inventory of the full set of results, including the four seasonal and 12 monthly situations, can be found in Brasseur *et al.* (1994).

In order to check the general consistency of the reconstructed fields, several verifications have been achieved with respect to prior knowledge. One critical test concerns the static stability of the water column: extensive experiments have shown that the procedure doesn't generate hydrostatic instability in the three-dimensional results if the original data profiles are stable. This statement clearly features the importance of a prior quality control of the data.

As mentioned earlier, the numerical parameters of the variational principle have been adjusted according to the statistics of the MED2 data set. Various sensitivity studies with respect to the decorrelation scale and the observational noise are described in Brasseur (1994). It has been verified that the results are nearly independent of the choice of L for values exceeding 40 km, while they exhibit a noticeable sensitivity with respect to the weight or, equivalently, to the observational noise. However, the confidence intervals on the statistics estimated from MED2 are sufficiently robust to keep this sensitivity within acceptable ranges (Brankart and Brasseur, 1996). In the same way, the choice of the first-guess field, which is required when norm spline interpolation is used, does not significantly affect the results. The comments reported here, which are valid for both variational or statistical methods, are the consequence of the quantity of data available for each analysis: the conclusions would certainly be different if highly scattered data representative of quasi-synoptic situations had to be considered instead of historical records.

The salinity distributions calculated at 10-m depth are illustrated in Fig. 11, comparing summer and winter conditions. The continuous increase of salinity from the Strait of Gibraltar to the eastern basin reflects the gradual modification of surface properties as Atlantic waters penetrate into the domain. The rather strong exchanges taking place at the air–sea interface are most likely responsible for this general trend: indeed, it is well known that the Mediterranean site can be considered as a concentration basin in which evaporation exceeds precipitation and river runoff (e.g. Bethoux, 1979; Garrett *et al.*, 1993). The same tendency was already detectable at a more global scale from the Levitus data set (Fig. 1).

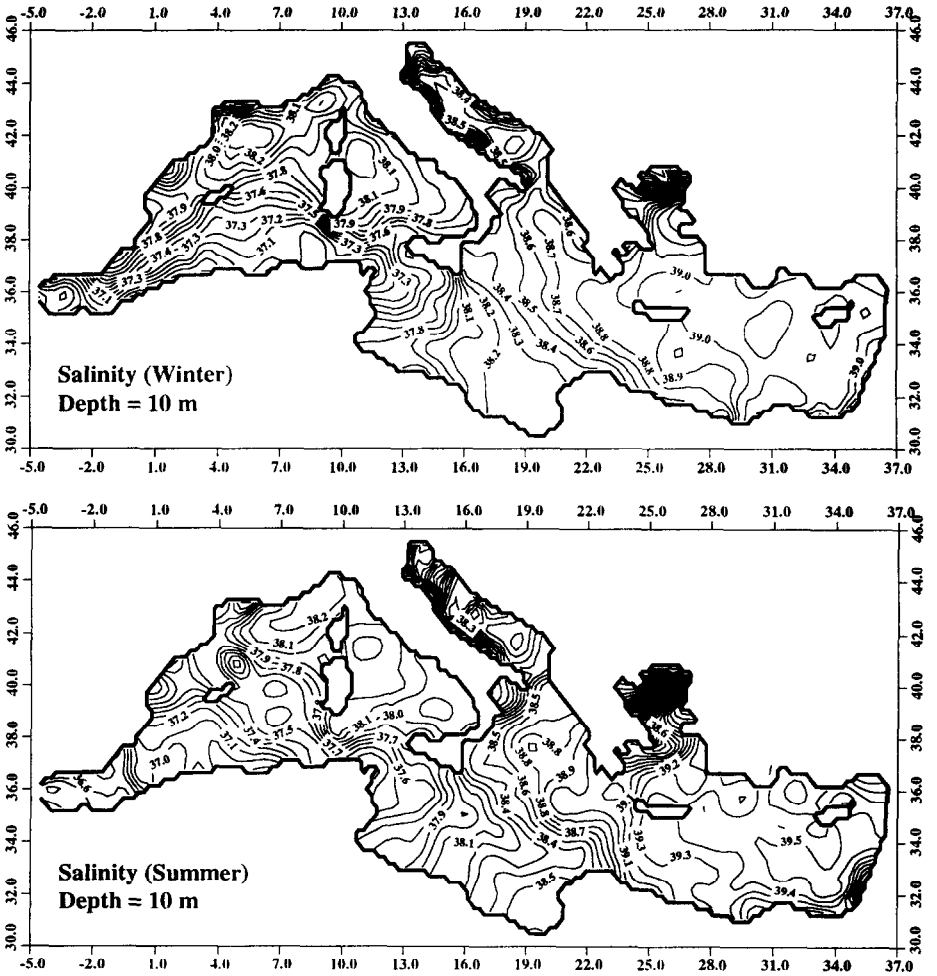

Fig. 11. Reconstruction of the salinity field from the MED2 data available at 10-m depth: comparison between winter and summer conditions.

Superimposed upon the global pattern, the salinity distribution of Fig. 11 reveals a series of sub-basin-scale gyres which had been evidenced previously in regional studies. The cyclonic gyre in the northwestern basin appears as the most energetic feature of the winter period. This cyclone is associated with deep water formation that typically occurs during February, in conjunction with strong atmospheric events (Gascard, 1978). The maximum salinity exceeds 38.3 over the region centred on the Gulf of Lions, in agreement with several surveys of MEDOC Group (1970). The process of deep convection typically starts with a "preconditioning" phase that corresponds to the homogenization of the water column within the gyre. As described later, the three-dimensional structure of the reconstructed fields accounts for this vertical homogenization fairly well. The trace of the cyclonic circulation associated with the preconditioning phase is clearly marked in Fig. 11, whereas it is almost absent from Fig. 1. As far as modelling is concerned, the MED2 reconstructed

fields will provide better initial conditions than the Levitus data, especially for numerical experiments designed to simulate deep water production.

The salinity in the Gulf of Lions is slightly attenuated in summer, while the distributions calculated in the eastern basin may reach values exceeding 39.4 during the same period: this fact suggests that the seasonal cycle of the surface salinity is out of phase between the eastern and the western basin. A careful examination of monthly fields confirms this seasonal evolution. According to the discussion of Malanotte-Rizzoli and Hecht (1988), the climatological wind patterns could provide some explanation for this. Indeed, the winter situation shows a mostly zonal wind field over the eastern Mediterranean, with the wind essentially blowing above the sea from Sicily to the Levantine basin and advecting humid air masses. The summer situation, however, indicates a mostly meridional wind field, blowing from Europe towards Africa: this continental regime, characterized by dry and warm air masses, results in more pronounced evaporation rates over the Levantine basin confirming our interpretation of the seasonal cycle.

In spite of the coarse resolution of the gridded fields (0.25°, in agreement with the correlation scale of 80 km), the Western Alboran Sea gyre can be quite well identified on the salinity distributions. Heburn and La Violette (1990) have reported the presence of a second anticyclonic gyre to the east of 3°W. However, the eastern gyre is known to be more intermittent than the western one; this intermittency could explain why its trace is strongly smoothed on our analyses.

One should also note the maximum salinity observed to the southeast of Corsica; this feature, which is reproduced on the four seasonal pictures, is suspected to be the site of a permanent cyclonic circulation developed in the northern sector of the Tyrrhenian Sea.

As a consequence of the low salinity waters originating from the Black Sea, the salinity abruptly decreases in the northern Aegean Sea, and more specifically in the vicinity of the Dardanelles Strait. Compared to the real ocean, the horizontal extension of this water mass is probably exaggerated in Fig. 11; a more local analysis, based on regional correlation scales, would probably lead to more realistic results in the northern Aegean Sea.

Because of surface heat fluxes, the summer and winter temperature distributions in the upper layer are totally contrasted (Fig. 12): one can notice a mean shift of about 9°C between the two seasons. During winter the thermal structure of the western basin is fairly homogeneous, especially in the northwestern area that extends from the Balearic Islands to the Ligurian Sea: in this region, the temperature at 10-m depth doesn't exceed 13°C. The coldest waters are found on the Italian side of the Adriatic Sea, within a thin coastal layer characterized by temperatures of about 9°C. The fields of Fig. 11 indicate that the salinity in this coastal region is also very weak. The strong cooling of these waters is probably due to the combined effect of the Pô river discharge and the Bura wind, which blows violently from the north during winter (Zore-Armanda and Gacic, 1987). In the Levantine basin, the cold core associated with the Rhode Gyre appears as the most remarkable feature: it has developed in a double-cell system between Crete and Cyprus during winter, while its trace on the summer fields is much less pronounced. Similar observations have been reported by other authors (e.g. Özsoy *et al.*, 1989). In the Alboran Sea, the trace of the western gyre on the salinity field corresponds to low temperature values during all seasons.

Generally speaking, the thermal field at 10-m depth is less structured during summer than during winter. This can be understood quite easily. During summer, any interaction or exchange occurring across the thermocline may result in severe local variations due to strong vertical gradients in temperature. By contrast during winter, the water column is

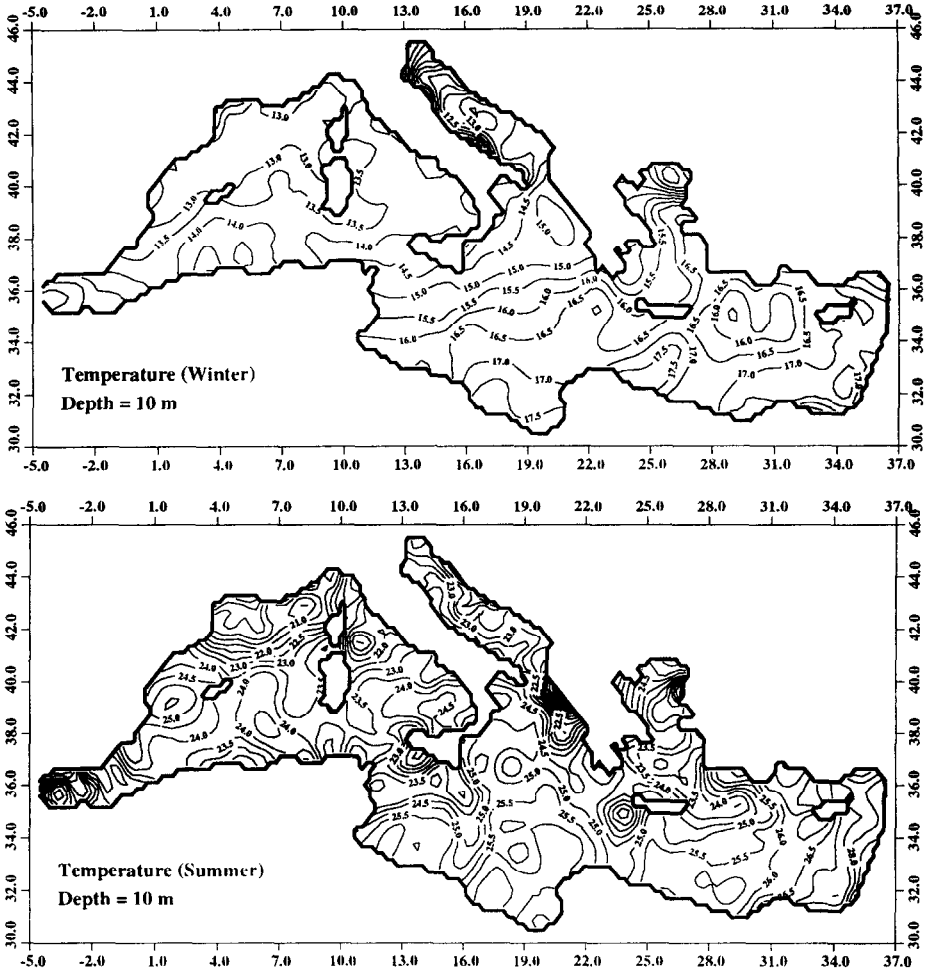

Fig. 12. Reconstruction of the temperature field from the MED2 data available at 10-m depth: comparison between winter and summer conditions.

much less stratified in temperature, and perturbations in the upper layer often have less dramatic effects.

Although most of our conclusions have been reported in the literature, some benefits can be gained from a precise and global assessment of SST fields through the seasonal cycle. Indeed, it is often argued that atmospheric fluxes are poorly known, including their parameterization into numerical models with active thermodynamics. In such situations, one can consider that appropriate analyses of *in situ* observations make up the best expected response of the model at the surface. In the context of the Mediterranean, one possible solution to reach this objective is to assimilate the MED2 reconstructed fields through the air–sea boundary condition, for instance using the parameterization suggested by Haney (1971). This approach has been followed by Beckers (1992) and Stanev and Friedrich (1991) in primitive equation models of the Mediterranean; obviously, the assimilation of

temperature data at the sea surface has significantly improved the thermal fields as well as the overall picture of the circulation.

At this stage however, only seasonal realizations of the thermal fields (and associated heat content) have been obtained, so that the annual cycle is poorly reproduced. With an improved data set, it will be possible to refine our representation of the typical annual cycle, using monthly distributions to compute month-to-month variations of heat and freshwater content. This might be useful for constraining air–sea flux calculations from COADS data (Garrett *et al.*, 1993) or atmospheric models.

The density field is readily computed from the temperature and salinity distributions of Figs 11 and 12, using the UNESCO state equation (Fig. 13). The similarities between the density and salinity fields during winter indicate that baroclinic processes are more substantially influenced by salinity than temperature. In the coastal zone, density gradients are intensified at the mouth of some important rivers where many data are systematically collected (e.g. the Rhône). This could be seen as an artefact of the analysis procedure, since the correlation scales are much shorter in the river plumes than in the open ocean. However, the horizontal density gradients are confined to the topmost layer (between the surface and 20-m depth), with marginal consequences on the baroclinic circulation.

In the above discussion, no distinction has been made between the regions where the data coverage is excellent (e.g. Gulf of Lions) and the regions almost void of data (e.g. Tunisian Shelf). However, the error maps shown in Fig. 14, which indicate the degree of reliability of the winter and summer analyses, should be checked before consulting the field distributions themselves. The error levels essentially reflect (i) the density of the data coverage and (ii) the quality of the measurements, identified as the ratio between the signal amplitude and the standard deviation of observational errors. The highest error levels are found in the southern sectors of the domain, with a maximum uncertainty located in the vicinity of the Tunisian Shelf. In addition to attesting to the quality of the reconstructions, such error maps could be very useful for the design of major operations at sea, for instance in the perspective of global observing experiments.

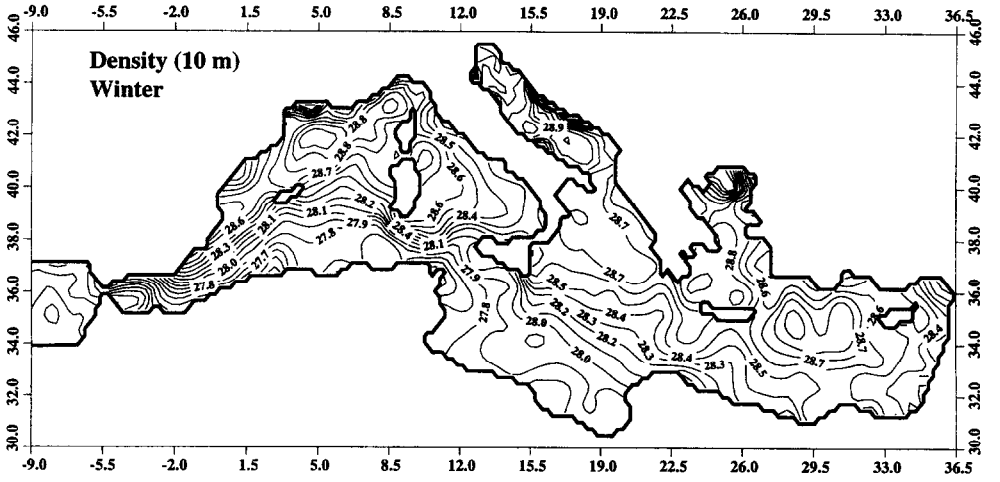

Fig. 13. Density field at 10-m depth during winter, as calculated from the temperature and salinity fields of Figs 11 and 12 and the UNESCO equation of state.

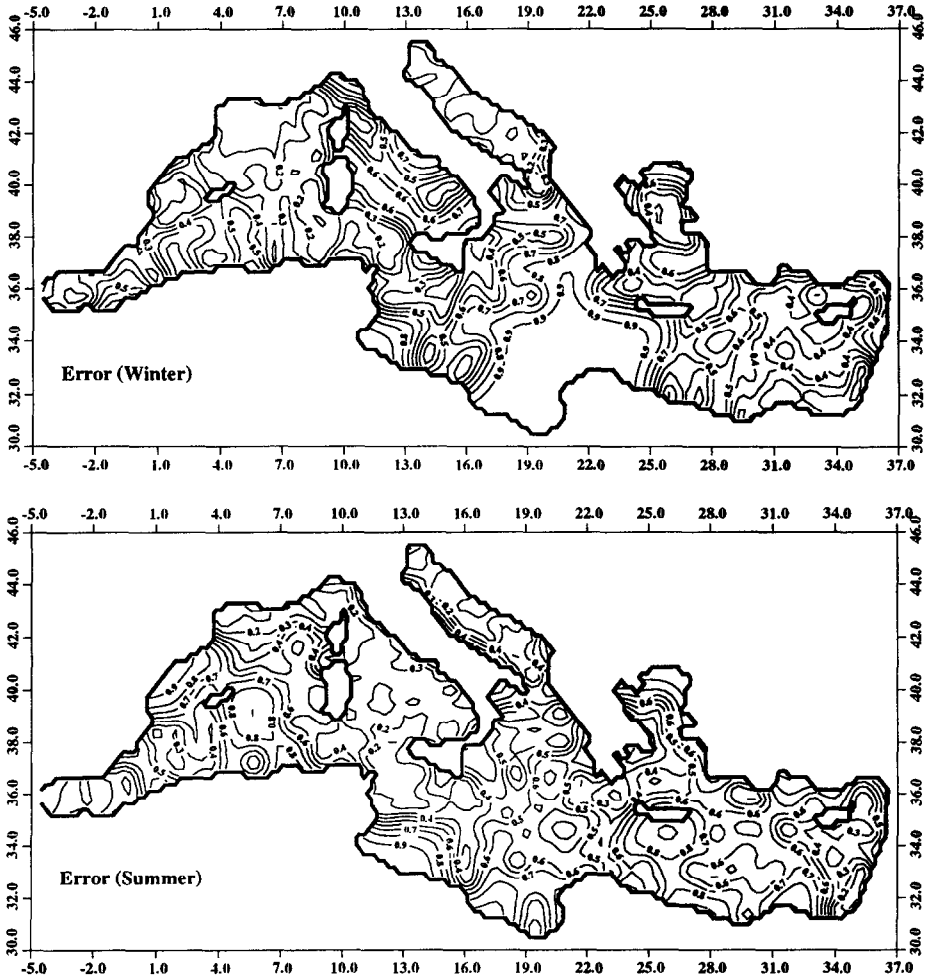

Fig. 14. Error maps (in standard deviation units) corresponding to the winter and summer salinity data sets (the stations available at 10-m depth have been considered for the calculation of error bars).

Even though some authors prefer to hide the field distributions in the sectors where errors exceed a certain value, we have kept the global fields in the figures, since the "gridded" data are supposed to serve as initial conditions for numerical models. In this respect figures should be provided everywhere, whatever the quality of the analyses (in regions void of data, our results approximately correspond to the first-guess field which is needed to perform the norm-spline analysis).

Traditionally, the vertical structure of the hydrological fields is described as the superposition of three water masses identified according to their formation sites. The upper layer is occupied by Modified Atlantic Water (MAW), which originates from the Strait of Gibraltar; at mid-depth, a fairly thick layer of Levantine Intermediate Water (LIW) propagates from the eastern to the western basin and gradually mixes with adjacent waters (the LIW body is formed during winter over the region surrounding the Rhode

Gyre); at depth finally, two voluminous reservoirs, separated by the Sicily Strait, are filled with Mediterranean Deep Water (MDW) produced during winter in the Gulf of Lions and in the Adriatic and Aegean seas. The distinctions among the three water masses are conventionally based on salinity ranges; in the western basin for instance, La Violette (1990) defines the interface between Atlantic and Mediterranean waters by the iso-salinity surface 38.45.

The vertical sections shown in Figs 15 and 16 (as well as other drawings reproduced in Brasseur *et al.* (1994)) depict this situation with a fairly good agreement. Figure 15 illustrates a zonal section at 37.5°N in the winter field. The westward spreading and progressive mixing of LIW with adjacent water masses is illustrated by the slow decrease of the salinity maximum encountered at about 400–500 m to the west of the Sicily Strait. The signature of Atlantic Water in the surface layer is much more clearly seen to the west of Sicily than in the eastern basin, suggesting that an important part of this water mass predominantly re-circulates in the western basin before crossing the Sicily Strait. The summer situation, not shown here, does not reflect substantial differences in the salinity structure.

Using advanced visualization techniques (Haus, 1993) or repeated cross-sections across the domain, thorough examinations of the three-dimensional fields reveal that LIW penetrates the Tyrrhenian basin after passing the Sicily Strait and then circulates around Sardinia and Corsica, in good agreement with the scheme described by Millot (1987). However, an important portion of LIW is also found off the Algerian coast, indicating that the path followed by intermediate water to reach the Strait of Gibraltar is not unique. This is confirmed by the meridional section drawn at 5°E (Fig. 16), since two maximum salinity values exceeding 38.5 psu are found: (i) at about 400-m depth along the African coast; and (ii) at about 500-m depth off the French coast. One can also check that these veins of water are characterized by local maxima of temperature, demonstrating clearly their Levantine origin.

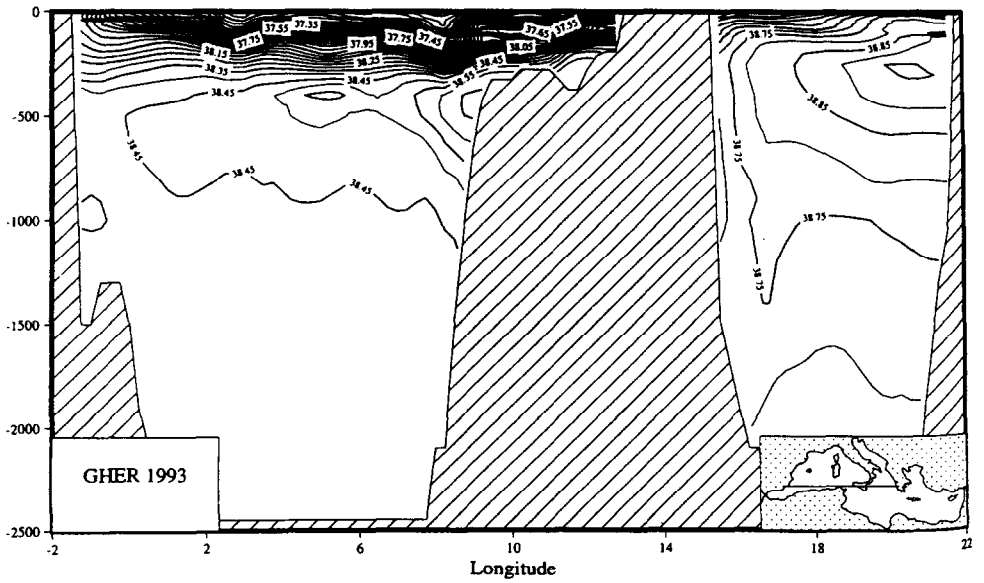

Fig. 15. Zonal section across the winter salinity field at 37.5°N, from the Spanish (left) to the Greek (right) coast.

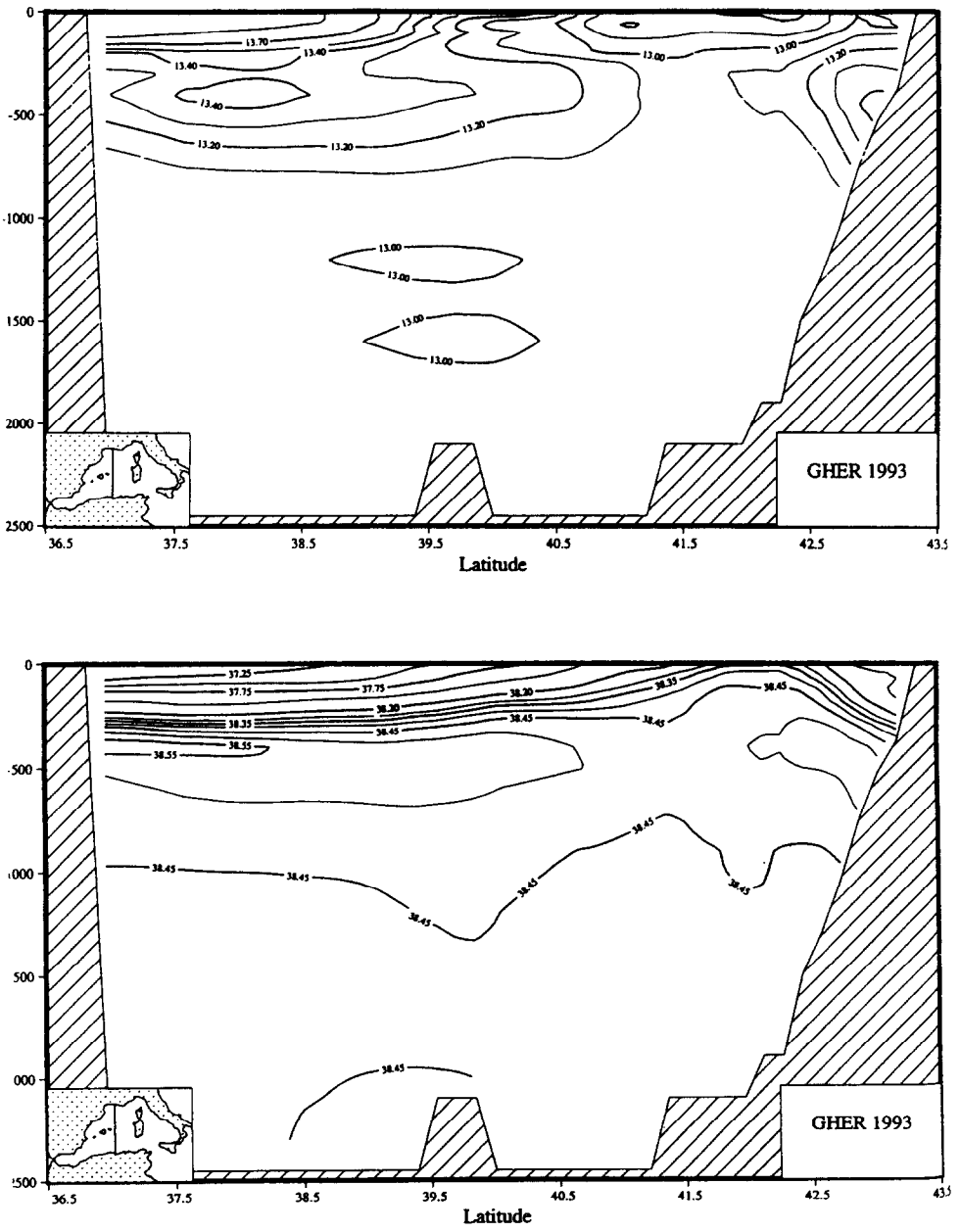

Fig. 16. Meridional sections across the winter temperature (upper) and salinity (lower) fields at 5°E, from the Algerian (left) to the French (right) coast.

Below 1000-m depth, the temperature and salinity fields are very homogeneous and display no significant seasonal variability. Since the deep hydrographic casts are much less frequent than the surface soundings, the best estimations of the deep water properties are obtained from a compilation of the four seasonal data sets. Figure 17 illustrates the temperature and salinity distributions in the deep water reservoirs (at 1000-m depth) resulting from the variational analysis of the global data set. As expected, horizontal gradients are evidently weaker than in the surface or intermediate layers. However, the geographical barrier created by the Sicily Strait introduces sharp transitions between the water properties in the eastern and western basins. The amplitudes of these transitions are much bigger than the typical variations within each basin, which suggests that the deep water pools are not directly connected.

A large variety of diagnostics can be derived from the three-dimensional temperature and

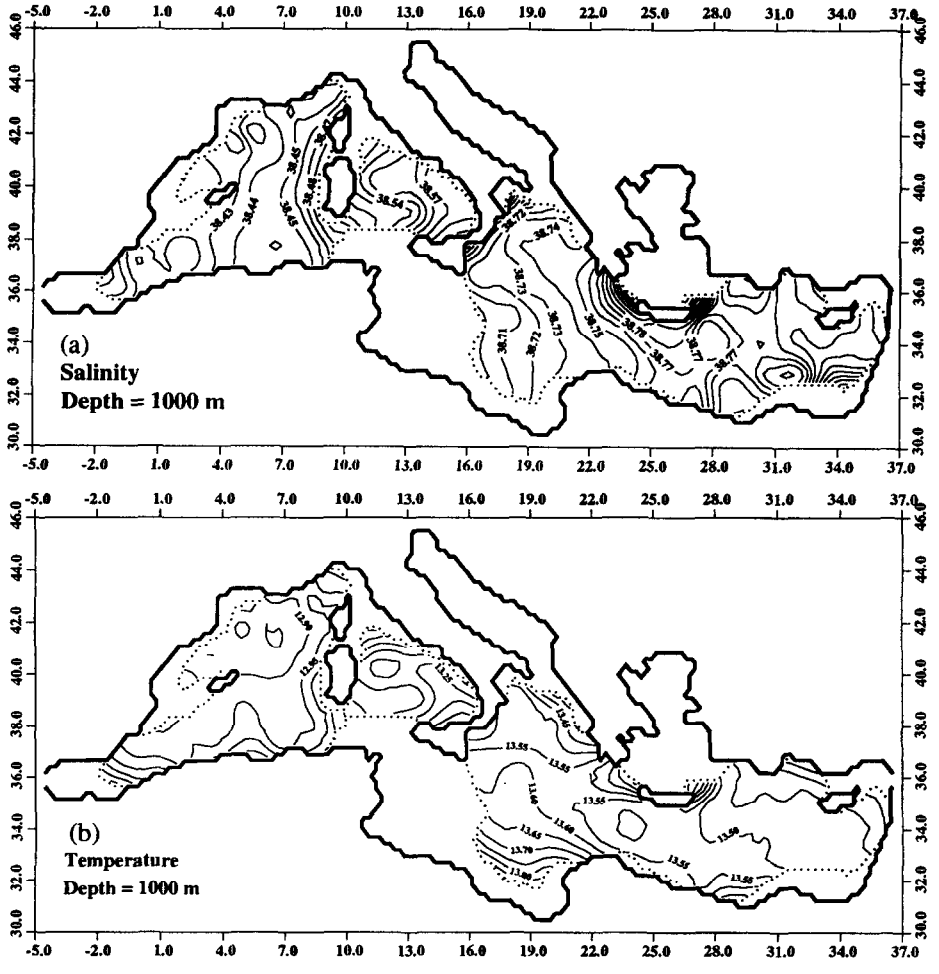

Fig. 17. Annual-mean distribution of (a) salinity and (b) temperature in the deep reservoirs (1000-m depth), as reconstructed from the MED2 data; the dotted line follows the 1000-m isobath.

salinity fields. Of course, the density ρ is the most trivial product, using the standard UNESCO equation of state as above. Another interesting diagnostic is the Brünt–Väisälä frequency N, defined by

$$N^2 = \frac{\partial b}{\partial z} \quad \text{and} \quad b = -g\frac{(\rho - \rho^*)}{\rho_0} \tag{15}$$

where b is the buoyancy, z is the vertical coordinate, ρ_0 is a reference (constant) density and $\rho^*(z)$ is a typical density profile. The potential vorticity is sometimes used instead of N to diagnose the water mass circulation (Haines and Wu, 1996). However, the Brünt–Väisälä frequency is a natural index of hydrostatic stability that appears in many turbulent closure schemes. Neutral stability corresponds to $N=0$, and hydrostatic instabilities occur for negative values of N^2. This index has been calculated from the temperature and salinity distributions over the whole domain in order to explore the seasonal evolution of the stratification in the upper layer and to check the stability of the results.

The Brünt–Väisälä frequency is represented in Fig. 18 along the meridional section crossing the Gulf of Lions (at 5°E). The contrast between the winter and spring stratifications is well marked, indicating the conditions that prevail when deep water formation occurs. The "preconditioning" situation described by Gascard (1978) is reflected in the winter section by the weakly stratified water column centred at 42°N. The deep water reservoir is then directly connected to the near surface layer. The "doming" effect, which is very typical of this process, is already detectable in the salinity section of Fig. 16. In spring, atmospheric heating through the air–sea interface reinstates the stratification of the surface layer, which is still reinforced during summer. Everywhere below 500 m, the stratification is very weak.

Since the three-dimensional density fields have been calculated over the whole domain, geostrophic velocities could be computed by integrating the thermal wind equations from a level where the velocity (or the pressure) is known. In the Mediterranean, the bottom topography and the processes are so complex that an assumption of level-of-no-motion is hard to justify. However, it is possible to determine this unknown reference with the assistance of an inverse model such as the one developed by Tziperman and Malanotte-Rizzoli (1991). Another possibility consists of using a free-surface, primitive equation model to adjust the sea surface elevation to prescribed density fields, and then to integrate the thermal wind equations from the surface down to the bottom. A detailed study of the dynamic adjustment of the velocity fields will form the subject of a forthcoming paper.

5 CONCLUSIONS

In this paper, we have presented the general framework set up to construct a reference climatology based on historical data in the Mediterranean Sea. Several existing data sets have been merged into a common file system that contains currently over 34,000 hydrographic profiles. In the near future, other regional data sets will be used to upgrade the MED2 data base and to fill in the gaps which still persist in some sectors.

Seasonal and monthly analyses of the data have been performed by a variational inverse (spline) method as an alternate to the standard objective scheme. This method has been demonstrated mathematically equivalent, but numerically more efficient, than the statistical procedure when huge historical data sets have to be processed. In addition, the spline

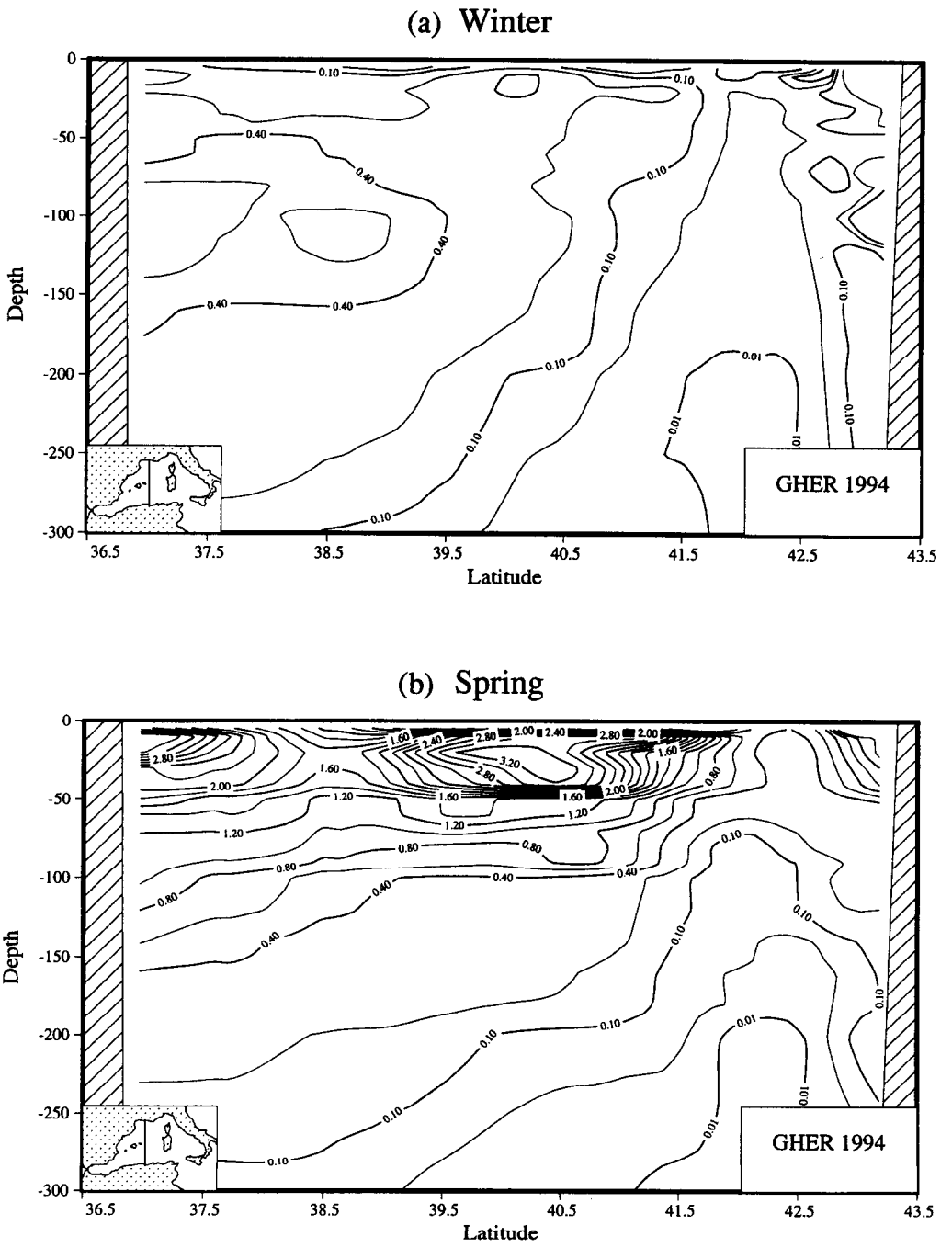

Fig. 18. Square of the Brünt–Väisälä frequency ($10^4\ s^{-2}$) in the upper 300-m layer, calculated from (a) winter and (b) spring fields in the same meridional section as in Fig. 16.

formulation has been shown to be more convenient for taking into account the geometrical peculiarities of the real Mediterranean domain.

The method has been routinely applied to produce an inventory of climatological analyses at seasonal and monthly scales. Some of the most significant results have been discussed and compared with existing knowledge, most often leading to good agreements with published studies. However, the principal interest of this work is to provide the basic support for advanced studies, such as diagnostic calculations, initialization of dynamical models, assimilation of hydrological data into primitive equation models, or planning of experimental surveys.

The gridded fields and the computer code for variational analysis have been prepared for general distribution among the scientific community. This work is part of the Mediterranean Oceanic Data Base (MODB) project, an initiative for data and information management undertaken under the leadership of the European *MArine Science and Technologies* programme. All available products (original hydrographic profiles, climatological analyses and computer code) can be downloaded to remote computers by anonymous ftp from the MODB data server (Internet address: modb.oce.ulg.ac.be). The computer code consists of several modules, including an automatic generator for triangular element grids and a rudimentary user's interface. The products are updated according to the availability of additional hydrological data.

Acknowledgements—The authors are greatly indebted to S. Levitus and A. Artegiani who provided them with part of the MED2 data. Special thanks are also due to N. Pinardi who strongly encouraged the authors in this enterprise and to anonymous referees for their constructive suggestions. This work was partially funded by the Commission of European Communities (grants MAS2 CT93.0055.CEE and MAS2.CT93.0075.BE), IBM and the National Fund for Scientific Research of Belgium.

REFERENCES

Beckers J. M. (1992) La Méditerranée Occidentale: de la Modélisation Mathématique à la Simulation Numérique. Ph.D. dissertation, Liège University, Belgium, 342 pp.

Bethoux J. P. (1979) Budgets of the Mediterranean Sea: their dependence on the local climate and on the characteristics of the Atlantic waters. *Oceanologica Acta*, **2**, 157–163.

Bethoux J. P. and D. Tailliez (1994) Deep-water in the western Mediterranean Sea, yearly climatic signature and enigmatic spreading. In: *Ocean processes in climate dynamics: global and mediterranean examples*, P. Malanotte-Rizzoli and A. R. Robinson, editors, NATO ASI Series, Kluwer, pp. 355–369.

Brankart J. M. and P. Brasseur (1996) Optimal analysis of *in situ* data in the western Mediterranean using statistics and cross-validation. *Journal of Atmospheric and Oceanic Technology*, **13**, 477–491.

Brasseur P. (1991) A variational inverse method for the reconstruction of general circulation fields in the northern Bering Sea. *Journal of Geophysical Research*, **96**, 4891–4907.

Brasseur P. (1994) Reconstitution de Champs d'Observations Océanographiques par le Modèle Variationnel Inverse: Méthodologie et Applications. Ph.D. dissertation, Collection des Publications de la Faculté des Sciences Appliquées No. 144, University of Liège, Belgium, 267 pp.

Brasseur P. and J. Haus (1991) Application of a 3-D variational inverse model to the analysis of ecohydrodynamic data in the northern Bering and southern Chukchi Seas. *Journal of Marine Systems*, **1**, 383–401.

Brasseur P., J. M. Brankart and J. M. Beckers (1994) Seasonal Variability of General Circulation Fields in the Mediterranean Sea: Inventory of Climatological Analyses. Progress report, University of Liège, Liège, Belgium.

Bretherton F. P., R. E. Davis and C. Fandry (1976) A technique for objective analysis and design of oceanographic instruments applied to MODE-73. *Deep-Sea Research*, **23**, 559–582.

Dhatt G. and G. Touzot (1984) *Une présentation de la méthode des éléments finis*, S. A. Maloine, editor. Collection Université de Compiègne, Paris, 543 pp.

Franke R. (1985) Thin plate splines with tension. *Computer Aided Geometric Design*, **2**, 87–95.

Gandin L. S. (1969) Objective Analysis of Meteorological Fields. Israel Program for Scientific Translations, Jerusalem, 242 pp.

Garrett C., R. Outerbridge and K.Thompson (1993) Interannual variability in Mediterranean heat and buoyancy fluxes. *Journal of Climate*, **6**, 900–910.

Gascard J. C. (1978) Mediterranean deep water formation baroclinic instability and oceanic eddies. *Oceanologica Acta*, **1**, 315–330.

Guibout P. (1987) *Atlas hydrographique de la Mediterranée*. IFREMER, 150 pp.

Haines K. and P. Wu (1996) Modelling the dispersal of Levantine Intermediate Water and its role in Mediterranean Deep Water formation. *Journal of Geophysical Research*, **101**(C3), 6591–6607.

Haney R. L. (1971) Surface thermal boundary conditions for ocean circulation models. *Journal of Physical Oceanography*, **1**, 241–248.

Haus J. (1993) Visualisation of real and simulation data in physical oceanography. Proceedings of the BCS Conference on "Animation and Scientific Visualisation", IBM Hursley Park, U.K.

Heburn G. W. and P. E. La Violette (1990) Variations in the structure of the anticyclonic gyres found in the Alboran Sea. *Journal of Geophysical Research*, **95**(C2), 1599–1613.

Hecht A., Z. Rosentroub and J. Bishop (1985) Temporal and spatial variations of heat storage in the eastern Mediterranean. *Israeli Journal of Earth Sciences*, **34**, 51–64.

Hopkins T. S. (1985), Physics of the sea. In: *Western Mediterranean*, R. Margalef, editor. Pergamon Press, Oxford, pp. 100–125.

Johnson C. (1990) *Numerical solution of partial differential equations by the finite element method.* Cambridge University Press, Cambridge, 297 pp.

La Violette P. E. (1990) The western Mediterranean circulation experiment (WMCE): Introduction. *Journal of Geophysical Research*, **95**(C2), 1511–1514.

La Violette P. E. (1994) Seasonal and interannual variability of the western Mediterranean Sea. Coastal and Estuarine Studies 46, AGU, Washington, D.C., 373 pp.

Levitus S. (1982) *Climatological atlas of the world ocean.* NOAA Prof. Paper 13, U.S. Government Printing Office, Washington, D.C., 173 pp.

Lorenc A. C. (1986) Analysis methods for numerical weather prediction. *Quarterly Journal of the Royal Meteorological Society*, **112**, 1188–1194.

Malanotte-Rizzoli P. and A. Hecht (1988) Large-scale properties of the eastern Mediterranean: a review. *Oceanologica Acta*, **11**, 323–335.

McIntosh P. C. (1990) Oceanographic data interpolation: objective analysis and splines. *Journal of Geophysical Research*, **95**(C8), 13529–13541.

MEDOC Group (1970) Observation of formation of deep water in the Mediterranean Sea, 1969. *Nature*, **227**, 1037–1040.

Millot C. (1987) Circulation in the western Mediterranean Sea. *Oceanologica Acta*, **10**, 143–149.

Millot C. (1994) Models and data: a synergetic approach in the western Mediterranean Sea. In: *Ocean processes in climate dynamics: global and Mediterranean examples*, P. Malanotte-Rizzoli and A. R. Robinson, editors. NATO ASI Series, Kluwer, pp. 407–425.

Ovchinnikov I. M., Y. A. Plakhin, L. V. Moscalenko, K. V. Negljad, A. S. Osadichii, A. F. Fedoseev, V. G. Krivosheja and K. V. Voitova (1976) *Hydrology of the Mediterranean Sea.* Hydrometeoizdat, Leningrad, 376 pp.

Özsoy E. and H. Güngör (1994) The northern Levantine Sea circulation based on combined analyses of CTD and ADCP data. In: *Data assimilation: tools for modelling the ocean in a global change perspective*, P. P. Brasseur and J. C. Nihoul, editors. NATO ASI Series I 19, Springer, Hiedelberg, Germany, pp. 135–165.

Özsoy E., A. Hecht and Ü. Ünlüata (1989) Circulation and hydrography of the Levantine Basin. Results of POEM coordinate experiments 1985–1986. *Progress in Oceanography*, **22**, 125–170.

Picco P. (1990) *Cimatologial atlas of the western Mediterranean.* ENEA Santa Teresa Centre, La Spezia, Italy, 224 pp.

POEM Group (1992) General circulation of the eastern Mediterranean Sea. *Earth-Science Reviews*, **32**, 285–308.

Provost C. (1987) The variational inverse method revisited. *Annales Geophysicae*, **5B**(3), 213–220.

Robinson A. R. and W. G. Leslie (1985) Estimation and prediction of oceanic fields. *Progress in Oceanography*, **14**, 485–510.

Robinson A. R., M. Golnaraghi, W. G. Leslie, A. Artegiani, A. Hecht, E. Lazzori, A. Michelato, E. Sansone, A. Theocharis and Ü. Ünlüata (1991) The eastern Mediterranean general circulation: features, structure and variability. *Dynamics of the Atmosphere and Oceans*, **15**, 215–240.

Rohling E. J. and H. L. Bryden (1992) Man-induced salinity and temperature increases in the western Mediterranean Deep Water. *Journal of Geophysical Research*, **97**(C7), 11,191–11,198.

Sasaki Y. (1970) Some basic formalisms in numerical variational analysis. *Monthly Weather Review*, **98**, 875–883.

Sasaki Y. (1971) A theoretical interpretation of anisotropically weighted smooting on the basis of numerical variational analysis. *Monthly Weather Review*, **99**, 698–707.

Stanev E. V. and H. J. Friedrich (1991) On the assimilation of climatological data by means of numerical circulation models, examplified for the Mediterranean Sea. *Oceanologica Acta*, **14**, 97–114.

Thiebaux J. (1975) Experiments with correlation representations for objective analysis. *Monthly Weather Review*, **103**, 716–727.

Tziperman E. and P. Malanotte-Rizzoli (1991) The climatological seasonal circulation of the Mediterranean Sea. *Journal of Marine Research*, **49**, 411–434.

de Veubeke F. (1974) Variational principles and the patch test. *International Journal of Numerical Methods in Engineering*, **8**, 783–801.

Wahba G. (1990) *Spline models for observational data.* CBMS–NSF Regional Conference Series in Applied Mathematics 59, Society for Industrial and Applied Mathematics, Philadelphia, Pennsylvania, 169 pp.

Wahba G. and J. Wendelberger (1980) Some new mathematical methods for variational objective analysis using splines and cross validation. *Monthly Weather Review*, **108**, 1122–1143.

Zienkiewicz O. (1977) *The finite element method in engineering science* (3rd edition). McGraw-Hill, New York.

Zore-Armanda M. and M. Gacic (1987) Effects of bura on the circulation in the North Adriatic. *Annales Geophysicae*, **5B**(1), 93–102.